

Modeling and Analysis of the Buckling Phenomena in the Homogeneous and Heterogeneous Biomembranes

by

Seyed Ali Madani Tonekaboni

A thesis
presented to the University of Waterloo
in fulfillment of the
thesis requirement for the degree of
Master of Applied Science
in
Mechanical Engineering

Waterloo, Ontario, Canada, 2013

© Seyed Ali Madani Tonekaboni 2013

I hereby declare that I am the sole author of this thesis. This is a true copy of the thesis, including any required final revisions, as accepted by my examiners.

I understand that my thesis may be made electronically available to the public.

Abstract

In this project, nonlinear behavior of biomembrane are modeled as heterogeneous elastic biological systems. In addition to the static behavior of the membranes, their dynamic behavior are modeled to be able to investigate time-dependency of the variables of the systems. Some of the available models are used and some new ones are developed to study static and dynamic analysis of monolayer and bilayer membranes as well as circular axisymmetric biomembranes. The presented models are developed based on the Euler-Bernoulli constitutive law and employed to investigate buckling phenomena in the membranes as one of the most important physical phenomena in biological environment.

Static and dynamic behavior of Buckling phenomenon in biological membranes are modeled. The static model results in nonlinear ordinary differential equation for one-dimensional approximation. In order to extend the model for circular membranes, the criteria of constant length in one-dimensional membranes is changed to constant surface. Moreover, tension-compression and bending springs are added to the model and employed to study buckling of biomembranes. Similar to the procedure of obtaining the equations of static large deformation of the membrane, the equations of motion of the membrane is obtained using free body diagram of an infinitesimal element of the membrane and employing Euler-Bernoulli constitutive law. Hence, nonlinear integro partial differential equations are obtained to model the dynamic behavior of the membrane. All of the equations, including static and dynamic ones, are changed to the dimensionless forms so that the results can be considered general and can be employed to analyze different systems with different properties.

The nondimensional equations of each part of the project are solved using different iterative and time-dependent schemes. The schemes are used to obtain the discretized forms of the equations. The discretized equations of all nodes of the domain, with due attention to the considered boundary conditions, are gathered in a matrix and the matrix solved to obtain the solution of the variables at each node and time stage.

The solutions obtained for different problems investigated in this project are employed to

illustrate variations of different dependent variables of the models with respect to the independent variables and parameters of the problems. As the important step to analyze the problems, different results of the problems investigated in the project are verified using the available information in literature. Membrane profile are obtained for different parameter values and external forces in the stationary condition. In addition, variation of maximum deflection and slope are studied with respect to the variation of different dimensionless parameters of the system. As a verification of the solution, the incompressibility of bilayer membrane is shown as well. Growth of different variables is shown with respect to time employing the solution of dynamic modeling of the membrane. As one of the important parts of this project, effects of heterogeneity on dynamic behavior of the membrane under buckling is investigated. The heterogeneous region is considered to have different material properties and its position is changed to also study the geometrical effects.

Acknowledgments

I would like to thank my supervisors, Professor Karttunen and Professor Daun who guided me throughout this work.

Dedication

I dedicate this work to my parents and many friends helped me in critical situations and encourage me to grow and do my work everytime in the best way. I dedicate it to my love...

Table of Contents

List of Tables	ix
List of Figures	x
1 Introduction and Background	1
1.1 Theoretical background	2
1.1.1 Elasticity	2
1.2 From cells to organs	5
1.3 Cell components	6
1.4 Biomembranes	8
1.5 Cell mechanics	17
1.5.1 Viscoelastic models of red blood cell	19
1.6 Membrane analysis	26
1.6.1 Simulation	27
1.6.2 Analytical investigations	30

2	Methods	34
2.1	Mathematical modeling	34
2.1.1	Static analysis of membrane	35
2.1.2	Static analysis of bilayer membrane	37
2.1.3	Dynamic analysis of membrane	39
3	Numerical procedure	43
3.1	Static analysis of membrane	43
3.2	Static analysis of bilayer membrane	44
3.3	Dynamic analysis of membrane	45
3.4	Convergence, grid-independence and verification of the solution	46
4	Results and discussion	48
4.1	Static analysis of membrane	48
4.2	Static analysis of bilayer membrane	52
4.3	Dynamic analysis of membrane	54
5	Conclusion	79
6	Outlook	81
	Appendix A Modeling of biomembrane using energy method	82
	Bibliography	90

List of Tables

1.1	Range of v^* for different biomembrane shapes [4].	13
1.2	Selected measurements of the apparent area compression modulus K_A of lipid bilayers and cell membranes [4].	16
1.3	Bending rigidity for selected lipid bilayers and cell membranes [4].	18
1.4	Given and estimated values of the two parameters and rate of strain for RBC.	26

List of Figures

1.1	(a)Schematic representation of lipid bilayer including protein and cholesterol (The picture is licensed under the Creative Commons license and can be found at http://www.functionalwellness.com/services/cholesterol-management/); (b)Fluorescent image of eukaryotic cytoskeleton; Nuclei are in blue, actin filaments in red and microtubules in green (The picture is licensed under the Creative Commons license and can be found at http://en.wikipedia.org/wiki/Cytoskeleton).	9
1.2	Schematic representation of glycerol (The picture is licensed under the Creative Commons license and can be found at http://en.wikipedia.org/wiki/Glycerol). The -OH at each branch is connected to a carbon atom.	10
1.3	Schematic representation of bilayer sheet, liposome and micelle from top left to top right. Different parts of phospholipid molecule are also shown in the bottom.	11
1.4	Packing constraints experienced by a typical amphiphile in four aggregates. By increasing a_0l_{hc} for the same volume, the structures change from spherical micelles (a); to cylindrical micelles (b); to bilayers (c) and finally to inverted micelles (d).	15
1.5	In-plane tension to a uniform plane; σ_x and σ_y are extensional stresses in the shown x and y directions, respectively.	15
1.6	Schematic representation of a surface with nonzero curvatures.	17

1.7	Mechanical model of the cell membrane used to describe the kinetics of the membrane breakdown [56]; k_1 and k_2 are two springs and η_1 and η_2 are two dashpots in the schematic model.	21
1.8	Schematic representation of the computer experiments (The picture is taken from [71]. Reproduced with permission from Nature). Left: By applying a force \mathbf{F} normal to the surface of the sphere its radius decreases from R_0 to its final radius R_f . Right: Microscopic detail of the triangulated surface model of a two-dimensional sheet (The details are available in [71]).	28
1.9	Buckled monolayer membrane using atomic simulation (Figure courtesy of Bin Liu, SoftSimu Group, University of Waterloo.).	30
1.10	Goldstone modes ($m = 1$). From top to bottom $n = 1$, $n = 2$ and $n = 3$. (The picture is taken from [21]. Reproduced with permission from American Physical Society).	33
2.1	A schematic model of an element of the membrane.	36
2.2	Schematic models of the springs considered between the nodes of the layers of the bilayer membrane (1 and 2 represent the first and second layers and i is the node number).	39
4.1	N_∞ versus number of iterations for different applied loads on a membrane with half length $L = 2/3$	59
4.2	Variation of difference of maximum slope based on two considered δx in a sequence with respect to $1/\delta x$	59
4.3	Comparison of the presented solution and energy-based solution [46] for $L = 2/3$	60
4.4	Comparison of the presented solution and energy-based solution [46] for $L = 4/3$	60

4.5	Membrane profiles after buckling for different applied loads and $L = 2/3$.	61
4.6	Membrane profiles after buckling for different applied loads and $L = 4/3$.	61
4.7	Variation of y_{max} and θ_{max} with respect to applied load for a membrane with half length $L = 1$.	62
4.8	Variation of y_{max} with respect to the position of the small softer part ($l_h = 1/5$) of the heterogenous membrane ($L = 1$) under different horizontal loads.	62
4.9	Variation of y_{max} with respect to the position of the small stiffened part ($l_h = 1/5$) of the heterogenous membrane ($L = 1$) under different horizontal loads.	63
4.10	y_{max} versus λ for a heterogenous membrane, heterogeneity located at the middle, with half length $L = 1$ under different horizontal loads.	63
4.11	profiles of circular membrane after buckling for different applied loads and $L = 2/3$.	64
4.12	profiles of circular membrane after buckling for different applied loads and $L = 4/3$.	65
4.13	Variations of θ_{max} , x_{max} and y_{max} with respect to P_x .	65
4.14	Variations of y_{max} and θ_{max} with respect to non-dimensional stiffness of the middle part of the membrane with length $l_h = 1/5$.	66
4.15	Profiles of the layers of the bilayer membrane with half length $L = 1/2$ and under applied load $P_x = 41$.	66
4.16	Profiles of the layers of the bilayer membrane with half length $L = 1/2$ and under applied load $P_x = 47$.	67
4.17	Energy of the bilayer mambrane versus γ using both continuum method of this project and energy method of [30].	67

4.18	Variation of F_x applied to the bilayer membrane with half length $L = 1/2$ with respect to γ using both continuum method of this project and energy method of [30].	68
4.19	Relative incompressibility error in the bilayer membrane with half length $L = 1/2$ under different applied buckling loads.	68
4.20	Variation of y_{max} with respect to time for a cantilever beam subjected to a step loading as verification of the dynamic model [74].	69
4.21	Variation of maximum deflection with respect to time for the monolayer membrane with half length $L = 4/3$ under different applied buckling loads.	69
4.22	Variation of maximum deflection with respect to time for the monolayer membrane with half length $L = 2/3$ under different applied buckling loads.	70
4.23	T_{steady} versus applied horizontal load P_x for the membrane with half length $L = 1$	71
4.24	T_{steady} versus dimensionless stiffness λ for the membrane with half length $L = 1$	71
4.25	Bode diagram of the monolayer membrane with half length $L = 1$. Magnitude (dB) and phase (deg) of y_{max} with respect to frequency of the system (rad/s)	72
4.26	Variation of T_{steady} of the membrane with half length $L = 1$ with respect to the beginning position of the heterogeneous part with $\lambda_h = 10/9$ and $l_h = 0.2$	73
4.27	Variation of T_{steady} with respect to the beginning position of the heterogeneous part with $\lambda_h = 9/10$ and $l_h = 0.2$	73
4.28	T_{steady} versus heterogeneous stiffness λ_h for the heterogeneous part located in the middle of the considered half membrane.	74
4.29	Variation of T_{steady} of the membrane with half length $L = 1$ with respect to the beginning position of the heterogeneous part with $\rho_h = 2\rho$ and $l_h = 0.2$	74

4.30	Variation of T_{steady} of the membrane with half length $L = 1$ with respect to the beginning position of the heterogeneous part with $\rho_h = 0.5\rho$ and $l_h = 0.2$.	75
4.31	T_{steady} versus heterogeneous density ρ_h for the heterogeneous part located in $a = 0.34$ of the considered half membrane.	75
4.32	Variation of T_{steady} of the membrane with half length $L = 1$ with respect to the beginning position of the heterogeneous part with $C_h = 0.5C$ and $l_h = 0.2$.	76
4.33	Variation of T_{steady} of the membrane with half length $L = 1$ with respect to the beginning position of the heterogeneous part with $C_h = 2C$ and $l_h = 0.2$.	76
4.34	T_{steady} versus heterogeneous density C_h for the heterogeneous part located in $a = 0.4$ of the considered half membrane.	77
4.35	Variation of T_{steady} of the membrane with half length $L = 1$ with respect to the beginning position of the heterogeneous part with $D_h = 0.5D$ and $l_h = 0.2$	77
4.36	Variation of T_{steady} of the membrane with half length $L = 1$ with respect to the beginning position of the heterogeneous part with $D_h = 2D$ and $l_h = 0.2$.	78
4.37	T_{steady} versus heterogeneous density D_h for the heterogeneous part located in $a = 0.34$ of the considered half membrane.	78

Chapter 1

Introduction and Background

The purpose of this project is to present new modeling and (static and dynamic) analysis procedure of monolayer and bilayer membranes in different conditions. The presented models are based on theory of elasticity. Therefore, a brief review of some of the related definition and problems in elasticity is primarily presented in this chapter. In addition, because of the importance of membranes in biological environments and the existence of some of their kinds just in these environments, it is helpful to know about the different physiological systems. Membranes play important roles as coverage of cells and cell organelles. Hence, in the introductory part of this project cells and cell organelles as well as characteristics of different kinds of membranes are briefly introduced. Therefore, we are going to briefly describe the general roles of cells in a biological system. After presenting these sections about elasticity and biological environments and the roles of biological membranes in these environments, some of the important articles and projects have been done in the area of membrane analysis as well as cell mechanics are briefly reviewed.

1.1 Theoretical background

In this section, a brief introduction to elasticity is presented to help us in understanding the next sections dedicated for reviewing some articles about mechanical modeling of cells and membranes. It can also help us to understand the modeling part of the project. Most of the analysis of the biomembranes have been done by now are based on energy-based methods and energy functions of the system which are described later. Because of the new procedure used in this project to study the buckling of biomembranes using elasticity theory, it seems necessary to review some of the related elasticity formulation and laws here. It should be noted that the descriptions and formulations presented here are based on the two important and well-known references in this area including *Theory of Elasticity* by Landau and Lifshitz [36] and another book with same name by Timoshenko and Goodier [67].

1.1.1 Elasticity

In order to introduce some basic laws and formulations in elasticity theorem, the basic ideas and formulations of linear elasticity are presented as well as the ways to extend it to more general concepts in nonlinear elasticity. In addition, some of the nonlinear laws and formulations are presented separately. There are two primary variables in this theorem including stress and strain tensors defined as follows

$$\begin{aligned} F_i &= \frac{\partial \sigma_{ij}}{\partial x_j} \\ u_{ij} &= \frac{1}{2} \left(\frac{\partial u_i}{\partial x_j} + \frac{\partial u_j}{\partial x_i} \right) \end{aligned} \tag{1.1}$$

where F_i is the force per unit volume vector, σ_{ij} is the stress tensor and u_{ij} is the strain tensor. Now, using these definitions the following relations can be obtained

$$\begin{aligned}
\sigma_{xx} &= \frac{E}{(1+\nu)(1-2\nu)} [(1-\nu)u_{xx} + \nu(u_{yy} + u_{zz})] \\
\sigma_{yy} &= \frac{E}{(1+\nu)(1-2\nu)} [(1-\nu)u_{yy} + \nu(u_{xx} + u_{zz})] \\
\sigma_{zz} &= \frac{E}{(1+\nu)(1-2\nu)} [(1-\nu)u_{zz} + \nu(u_{xx} + u_{yy})] \\
\sigma_{xy} &= \frac{E}{(1+\nu)}u_{xy}, \quad \sigma_{xz} = \frac{E}{(1+\nu)}u_{xz}, \quad \sigma_{yz} = \frac{E}{(1+\nu)}u_{yz}
\end{aligned} \tag{1.2}$$

and conversely they can be written as

$$\begin{aligned}
u_{xx} &= \frac{1}{E} [\sigma_{xx} - \nu(\sigma_{yy} + \sigma_{zz})] \\
u_{yy} &= \frac{1}{E} [\sigma_{yy} - \nu(\sigma_{xx} + \sigma_{zz})] \\
u_{zz} &= \frac{1}{E} [\sigma_{zz} - \nu(\sigma_{xx} + \sigma_{yy})] \\
u_{xy} &= \frac{1+\nu}{E}\sigma_{xy}, \quad u_{xz} = \frac{1+\nu}{E}\sigma_{xz}, \quad u_{yz} = \frac{1+\nu}{E}\sigma_{yz}
\end{aligned} \tag{1.3}$$

where the all equations are presented in Cartesian coordinates. Now, the equations of equilibrium for isotropic solid bodies can be written as follows using both stress and strain tensorial terms

$$\begin{aligned}
\frac{\partial \sigma_{ik}}{\partial x_k} + F_b &= 0 \\
\frac{E}{2(1+\nu)} \frac{\partial^2 u_i}{\partial x_k^2} + \frac{E}{2(1+\nu)(1-2\nu)} \frac{\partial^2 u_l}{\partial x_i \partial x_l} + F_b &= 0
\end{aligned} \tag{1.4}$$

These general equations can be simplified in the two related problems (to our project) including bending of plates and rods. In the case of small bending of the plate, we have on both surfaces of the plate $\sigma_{xz} = \sigma_{yz} = \sigma_{zz} = 0$. Hence, the following equations can be obtained using the general stress tensorial terms of Eq.(1.2).

$$\begin{aligned}
\frac{\partial u_x}{\partial z} &= -\frac{\partial u_z}{\partial x} \\
\frac{\partial u_y}{\partial z} &= -\frac{\partial u_z}{\partial y} \\
u_{zz} &= -\sigma \frac{(u_{xx} + u_{yy})}{(1 - \sigma)}
\end{aligned} \tag{1.5}$$

In the presented equations, u_z can be replaced with sufficient accuracy by $\zeta(x, y)$ as the vertical displacement of the pints located in the neutral surface. So we have

$$u_x = -z \frac{\partial \zeta}{\partial x}, \quad u_y = -z \frac{\partial \zeta}{\partial y} \tag{1.6}$$

Therefore, all the components of the strain tensor can be determined as follows

$$\begin{aligned}
u_{xx} &= -z \frac{\partial^2 \zeta}{\partial x^2}, \quad u_{yy} = -z \frac{\partial^2 \zeta}{\partial y^2}, \quad u_{xy} = -z \frac{\partial^2 \zeta}{\partial x \partial y} \\
u_{xz} &= u_{yz} = 0, \quad u_{zz} = \frac{\sigma}{1 - \sigma} s \left(\frac{\partial^2 \zeta}{\partial x^2} + \frac{\partial^2 \zeta}{\partial y^2} \right)
\end{aligned} \tag{1.7}$$

By employing the variational method [36] and some calculations, the following equation can be obtained as the equation of equilibrium for a plate bent by external forces.

$$D \Delta^2 \zeta - P = 0 \tag{1.8}$$

where D is called the *flexural* or *cylindrical* rigidity, P represents external forces apply on the plate and $\Delta \equiv \partial^2/\partial x^2 + \partial^2/\partial y^2$ is here the two dimensional Laplacian. The procedure of obtaining the equations for some kinds of boundary conditions can be found in [36].

Some of the important formulations of small deflection of straight Euler-Bernoulli beam are also presented here to help us become familiar with the foundations of the ideas used in the mathematical procedures of this project. The different stress and strain tensorial

elements should satisfy the following equations in equilibrium

$$\begin{aligned}
 u_{zz} = \frac{\partial u_z}{\partial z} = \frac{x}{\rho}, \quad \frac{\partial u_x}{\partial x} = \frac{\partial u_y}{\partial y} = -\frac{\nu x}{\rho} \\
 \frac{\partial u_z}{\partial x} + \frac{\partial u_x}{\partial z} = 0, \quad \frac{\partial u_x}{\partial y} + \frac{\partial u_y}{\partial x} = 0, \quad \frac{\partial u_y}{\partial z} + \frac{\partial u_z}{\partial y} = 0
 \end{aligned}
 \tag{1.9}$$

where ρ is the radius of curvature of the neutral surface.

In order to extend the presented equations for linear elasticity to the nonlinear one, we can use two different methods. The first one is to use perturbation theorem and obtain higher order equations using the fundamental ones. The second one, also used in this project, is to write the equations basically without any assumption to simplify the problem.

1.2 From cells to organs

As the foundation of all functions and organisms on Earth, cells play an important role in nature [58]. They are the smallest units of life and as biological systems consists of different components. Cells can exist as solitary or as a unit of a multicellular organism. All of multicellular organisms have four levels of organization: cells, tissues, organs, and systems [58]. All of these systems have their own mechanical properties affects also the higher levels. As an example, the elastic properties of cells determine the mechanical behavior and characteristics of the related tissues. A brief information about these levels can help us to understand different effects of each level on the related higher levels.

Tissues are constructed from groups of cells with similar structures and functions. They can be categorized into four primary types including *epithelial*, *connective*, *muscular*, and *nervous* [58]. These tissues are described briefly to show their role and differences:

- **Epithelial tissues** cover surfaces throughout the body and made up of special cells for exchanging materials. "Epithelial cells are joined together very tightly to form epithelial sheets cover and line various organs" [58]. They are boundaries of organs separate them from their external environment. Because they are in the surface

of the organs such as the interior of vascular system in our body, their mechanical properties specially their resistance to shear and surface forces are so important.

- **Connective tissues** connect, support, and separate different organs of the body. Instead of large numbers of cells, they have relatively few ones scattered throughout a large environment of extracellular materials [58].
- **Muscular tissues** consist of cells and proteins to do their primary roles, *contraction*, *motion* and *force generation* in different parts of the body [58]. They have more strength with respect to the connective tissues because of their roles. They should be able to resist the smooth or sudden contractions. In addition, they have this ability to produce large forces depending on their volume and compactness [58].
- **Nervous tissues** consist of neurons specialized to support the nervous system's functions. Neurons are long and thin cells initiate and transmit electric pulses [58] throughout the body to connect brain and organs of the body.

Organs are collections of two or more types of tissues organized to serve a common function or functions [58]. Organs can also organized into organ systems to perform particular functions required for survival of the whole body.

Now, let us explain cell components to be aware more about this primary unit of life on Earth.

1.3 Cell components

Although individual cells are just small units in different levels of organization, they are highly complicated entities and contain different components are introduces and briefly described here. Living cells an be generally categorized into two general types [14]: *eukaryotic* cells, as units of higher organisms, and *prokaryotic* cells, such as bacteria. In order to understand mechanical modelings of cells and their organelles, it is necessary to know

the subsystems exist in cells. The basic structural elements are the same including membranes (fluid sheets) enclose the cells and their compartments and networks of filaments which maintain the cells shapes and help organize their contents.

- **Membrane** or cell wall envelopes the cell body and made of up lipids. The lipids construct bilayer so that each layer has approximately 2nm thickness and the total bilayer thickness is 4–5nm [4]. The lipid bilayers are interspersed by a heterogeneous structure of globular proteins (Fig.(1.1))[66]. They are permeable covering of cells and their organelles to separate them from their surrounding. In the next section, different characteristics of biomembranes and their roles in the body are described. The structural properties of the membrane are based on their specific role as coverage of the cells. They play important roles as impermeable coverage to prevent freely exchanging the interior contents of the cell with its environment. In addition, its capability for self-assembly and repair are so important for the cells [4]. They are so thin because their tensile strength is less important and usually the cytoskeleton determines the strength of the cells [4]. It is described later in this chapter that because of the special geometry and strength of the biological membranes, buckling is an important effect happening in these systems.
- **Cytoskeleton** consists of long rod-shaped molecules [4] attached to one another and to other organelles by connecting molecules that can adopt a remarkable range of configurations (Fig.(1.1)). They also
 - establish and maintain the shape of the cell
 - allow the cell to move by changing the cell shape (the process of locomotion)
 - provide mechanical strength and integrity

which affect strongly the mechanical properties and behavior of the cells [14, 4]. There are three types of filaments in cytoskeleton including actin filaments (7 – 9nm in diameter), intermediate filaments (10 nm in diameter), and microtubules (approximately 24 nm in diameter). The interaction between filaments has an important

effect on mechanical behavior [4]. Because of the physical properties of each kind of filaments, they have different mechanical roles in cells. As an example actin filaments and microtubules mostly resist to tensions and compression, respectively. These differences let the cells to move, change their shapes and play their role in the related environment.

Most of the studies about the mechanical properties of the cells and organelles have been dedicated to red blood cell [6, 9, 20] because of its special properties. They navigate through narrow capillaries in animal bodies and need to undergo rapid, reversible deformations. Therefore, its special cytoskeleton provides mechanical stability necessary to withstand the forces during in the circulatory environment.

The descriptions about other organelles of the eukaryotic cells and more details about the mentioned organelles are provided in literature [66, 14, 68].

1.4 Biomembranes

Biological membranes act as envelopes to surround the cell separating its internal and external environment. In addition, organelles have membranes as their boundaries which provide surfaces for the localization of metabolic enzymes, transport proteins, receptors, and various substrate [37]. In (1972), Singer and Nicholson proposed the fluid-mosaic model for the biomembranes. Biological membranes are fluid bilayer mostly including lipids and proteins. Although 50 percent of a biological membrane can be composed of proteins [1], structure mostly determined by the self-assembly of lipids.

The chemical, biological, physical and mechanical aspects of biomembranes as one of the important compartments in animal and human bodies have been investigated. Now, let us describe briefly the chemical composition of the membranes before explaining their physical and mechanical behavior and self-assembly procedures.

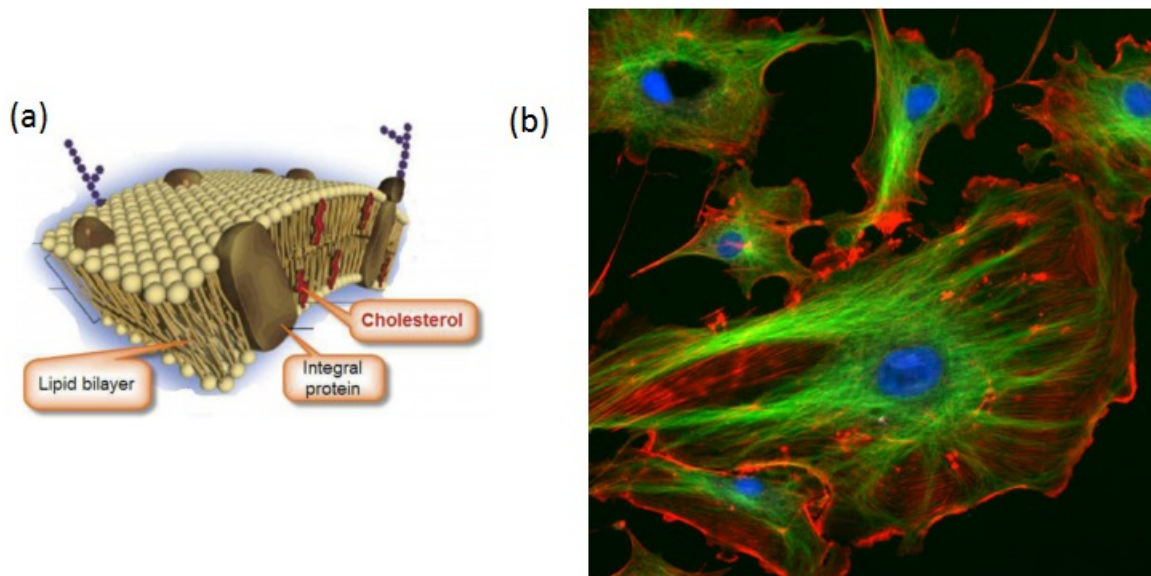


Figure 1.1: (a)Schematic representation of lipid bilayer including protein and cholesterol (The picture is licensed under the Creative Commons license and can be found at <http://www.functionalwellness.com/services/cholesterol-management/>); (b)Fluorescent image of eukaryotic cytoskeleton; Nuclei are in blue, actin filaments in red and microtubules in green (The picture is licensed under the Creative Commons license and can be found at <http://en.wikipedia.org/wiki/Cytoskeleton>).

Chemical composition of biomembranes

As the main structural components of biomembranes, details of phospholipids are presented here. Two main building blocks of lipids are *glycerol backbone* and *fatty acids* [68]. Glycerol is a small molecule contains three carbon and three hydroxyl groups (Fig.(1.2)). Different properties of fatty acids such as existence of double bonds, length of the carbon chain and being saturated or unsaturated are the most effective factors on determining the physical and mechanical properties of the related lipid [68]. The brief descriptions presented about lipids and their components can be helpful to understand the characteristics of different membrane lipids in the biological point of view which is not the concern of this project.

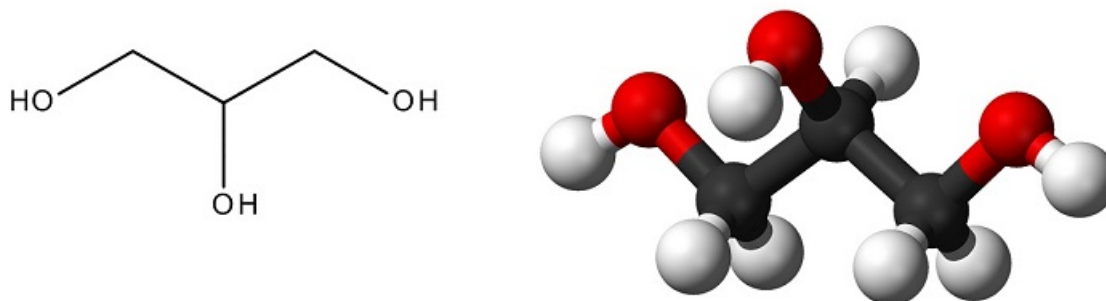


Figure 1.2: Schematic representation of glycerol (The picture is licensed under the Creative Commons license and can be found at <http://en.wikipedia.org/wiki/Glycerol>). The -OH at each branch is connected to a carbon atom.

Physical properties and self assembly of biomembranes

The interaction of lipids with water is an important parameter determines the self-assembly and physical behavior of biomembranes. All of the biological environments contain water such as intracellular environments, blood, etc. In order to investigate the interaction with water, their chemical components can be categorized into *hydrophilic* water-loving and *hydrophobic* or water-avoiding parts [68]. In phospholipid, there is a hydrophilic head group (Phosphate) and hydrophobic tails (hydrocarbon chains). This dual nature of phospholipids make them amphiphilic molecules [4].

In the interaction of oil an water, amphiphilic oil molecules arrange so that their hydrophilic head group has an interaction with water. On the other hand, their hydrophobic tails try to embeds in the oil environment (Fig.(1.3)) [4]. If we have a boundary between two areas of oil and water, the boundary lipid molecules can rearrange themselves so that their head groups be in contact with water in the boundary and their hydrophobic tails remain in the oily region, the phenomena happens when there is some oil in a glass of water. However, there is a big difference in arranging lipid molecules to form biological membranes because of existence of water on both sides of the boundary. As it is described before, biomembranes are thin boundaries separate intracellular and extracellular environ-

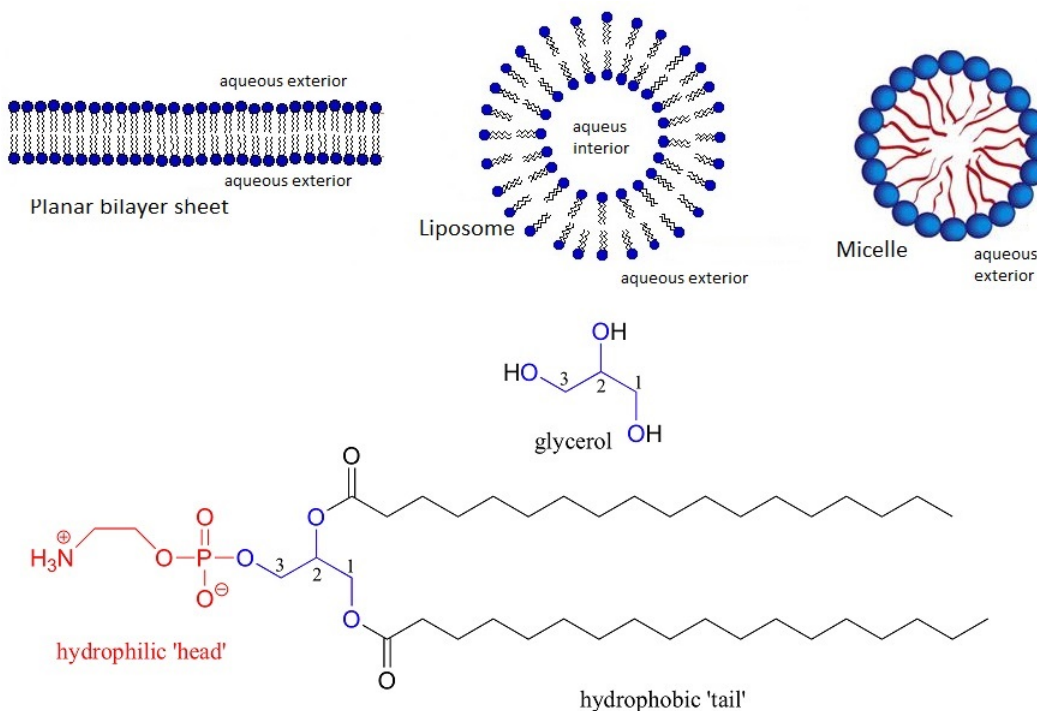


Figure 1.3: Schematic representation of bilayer sheet, liposome and micelle from top left to top right. Different parts of phospholipid molecule are also shown in the bottom.

ments or their organelles from intracellular region. Hence, almost always there is water on both sides of the biomembranes. Phospholipids can also form other structures such as micelles and liposomes [68]. Different structures of phospholipids including micelles (spherical monolayer membrane), liposomes (spherical bilayer membranes) and bilayer sheets which construct outer coverage of cells and its organelles are presented in Fig.(1.3). The differences between the shapes and curvatures of the shown systems as the important structural characteristics are based on the competition of the energy and entropic terms in free-energy function described later. There is water in both sides of bilayer sheet. The interior and exterior environments of liposomes are aqueous as well in contrast with micelles which their interiors are oily. Liposomes and micelles can be used as vehicles in gene therapy to deliver genes in the targeted cells [68]. Let us present the formation of different structures

in wet environment based on the concentration of fatty acids in the system.

The hydrophobic tails of the phospholipids contains two branch of hydrocarbon chains. In many biological phospholipids, one of the branches is saturated, all bonds are single, and the other one has a C – C double bond [4]. The existence of this double bound results in formation of different conformations. In biological layered structures, the single bond chains (saturated one) tend to straighten out through steric interactions with its neighbors. In contrast, there is a permanent kink in the other branch generated by the double bond, make the dense packing of phospholipids more difficult and reduce the in-plane viscosity of bilayer. As it is described, there is not only one lipid in the biomembranes and their hydrocarbon chains can be different as a cause of diversity of the lipids as a structural components of bilayers [4]. The chain lengths are mostly between 15 to 18 carbon atoms which is based on lipid concentration and operating temperature of the cell. The range of the membrane thicknesses is in nm which is much less than micron range for cell and organelles dimensions. Each hydrocarbon chain has between 15 – 18 carbon atoms and is approximately 2 nm in length resulting in total bilayer thickness of 4 – 5 nm. The mean cross-sectional area of a single chain is about 0.2 nm^2 , while the average surface area per lipid is $4 - 7 \text{ nm}^2$ for most membrane lipids [44]. There are also proteins and carbohydrates have different dimensions (lengths and area). The proteins of the bilayer membrane act mostly as channels for transferring the materials between intracellular and extracellular environments. They are longer than thickness of the bilayer to be able to easily do their work [4]. If we consider a pure lipid bilayer can be considered as a homogeneous membrane, these proteins and carbohydrate change it to a heterogeneous system. These heterogeneities have important effects on the physical and mechanical behavior of the membranes investigated in this project.

Formation of structures like micelles is based on the competition between the two terms defines free-energy $F = U - TS$ [4]. Entropy is decreased in this process based on decreasing the degrees of freedom of the system. Hence, it causes dispersion of the molecules. On the other hands, the molecules prefers to directly interact with each other based on the energy term. Therefore, there is a competition between these terms resulting in different

structures in every condition.

As it is mentioned before, there are different shapes possible for biomembranes. Hence, there should be a parameter to categorize the membranes. Let us consider a geometrical parameter for this purpose as follows [4]

$$v^* = \frac{v_{hc}}{a_0 l_{hc}} \quad (1.10)$$

where v_{hc} and l_{hc} are volume and maximum chain length of single saturated hydrocarbon chain, respectively, and a_0 is the average surface area occupied by the head group of the amphiphile.

Table 1.1: Range of v^* for different biomembrane shapes [4].

Biological membrane shape	Range of v^*
Spherical micelles	$v^* \leq 1/3$
Cylindrical micelles	$1.3 < v^* \leq 1/2$
Bilayers	$1/2 < v^* \leq 1$
Inverted micelles	$1 < v^*$

Different possible structures of lipids are classified in Table 1.1 based on the range of this parameter. These structures are also shown in Fig.(1.4). It is clearly shown that the shapes are formed based on the ranges of the defined parameter v^* . Each of these membrane have physical and mechanical properties of their own. Because of the importance of compression and bending resistance and focus of this project on the buckling phenomena in biomembranes, they are described here.

Similar to every macroscopic or microscopic membranes, different forces can be applied on the biomembranes such as compression or tension (Fig.(1.5)). For the plate shown in this figure, the in-plane elements of strain tensors can be written as [4]

$$u_{xx} = u_{yy} = \sigma (2/9K_V + 1/6\mu) \quad (1.11)$$

where K_V and μ are the volume compression and shear modulus in three dimensions, respectively [4]. In the presented relation, u_{xx} and u_{yy} are two dimensional strains defined as deformation per initial length [67]. In addition, σ is the stress as the normal force to the surface divided by the related surface [67]. It is also assumed that $\sigma_{xx} = \sigma_{yy} = \sigma$. We can define a two-dimensional tension as $\tau = \sigma t$ (t is the thickness of the considered plate) in the case of two-dimensional deflection. Therefore, based on the definition of the area compression modulus $\tau = K_A (u_{xx} + u_{yy})$, the following relation can be easily found

$$K_A = tK_V (4/9 + K_V/3\mu) \quad (1.12)$$

Because of the possibility of measuring the surface tension of water + amphiphile interface γ , it is useful to obtain a relation between area compression modulus K_A and surface tension. The energy of the system is [4]

$$E = 2\gamma a_0 + (\gamma/a) (a - a_0)^2 \quad (1.13)$$

where a is the mean interface area occupied by an amphiphile and a_0 is the value in which the energy is minimized in equilibrium condition. Hence, the elastic energy density can be written as $\gamma [(a - a_0)/a_0]^2$ which is equal to $K_A/2 \cdot (u_{xx} + u_{yy})^2$ where $u_{xx} + u_{yy} = (a - a_0)/a_0$. It can be concluded from these relations that for a monolayer membrane $K_A = 2\gamma$ and for a bilayer membrane $K_A = 4\gamma$.

Apparent values of K_A for some pure lipid bilayers are presented in Table 1.2. These values are obtained from the slope of stress-strain diagram of the different experimental techniques used to obtain the mechanical and physical properties of the membranes. The presented apparent moduli are different from the real values because of change in intramolecular separation as well as fluctuations in the system can be found in details in [4].

Generally, amphiphile molecules resist to change their positions resulting in different resistance of the system. In addition to compression or tension resistance is described before, the biomembranes have bending resistance. It can be easily seen that when we

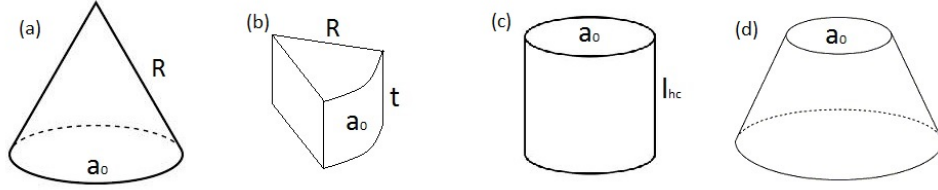


Figure 1.4: Packing constraints experienced by a typical amphiphile in four aggregates. By increasing $a_0 l_{hc}$ for the same volume, the structures change from spherical micelles (a); to cylindrical micelles (b); to bilayers (c) and finally to inverted micelles (d).

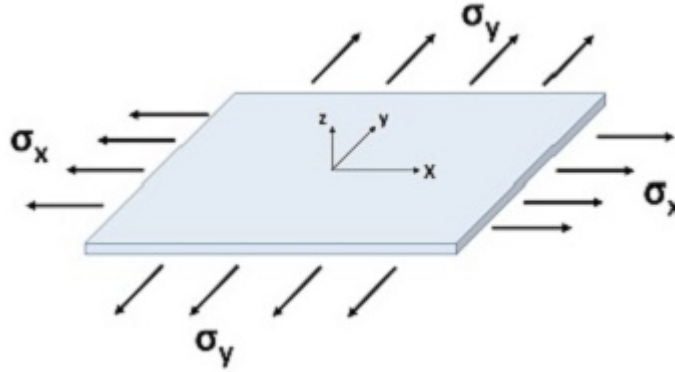


Figure 1.5: In-plane tension to a uniform plane; σ_x and σ_y are extensional stresses in the shown x and y directions, respectively.

want to bend a rod, more curvature of the system need more bending force and moment we should apply on it. Therefore, the bending resistance of the systems have been developed based on their curvatures. Any surface has two principle curvatures $C_1 = 1/R_1$ and $c_2 = 1/R_2$ in three dimensions (Fig.(1.6)). By employing these principle curvatures, two other curvatures can be defined [25] called mean curvature equal to $C_1/2 + C_2/2$ and Gaussian curvature equal to $C_1 C_2$. Thus, the energy density function \mathcal{F}

$$\mathcal{F} = (\kappa_b/2) \cdot (1/R_1 + 1/R_2)^2 + \kappa_G / (R_1 R_2) \quad (1.14)$$

Table 1.2: Selected measurements of the apparent area compression modulus K_A of lipid bilayers and cell membranes [4].

Membrane	T(c)	Apparent K_A (J/m^2)	Reference
diAPC	15	0.057 ± 0.014	Needham and Nunn, (1990)
	18	0.135 ± 0.020	Evans and Rawicz, (1990)
	21	0.183 ± 0.008	Rawics <i>et al.</i> , (2000)
diGDG	23	0.160 ± 0.007	Evans and Rawicz, (1990)
diMPC	21	0.150 ± 0.014	Rawicz <i>et al.</i> , (2000)
	29	0.145 ± 0.010	Evans and Rawicz, (1990)
	30	0.14	Koenig <i>et al.</i> , (1997)
diOPC	21	0.237 ± 0.016	Rawicz <i>et al.</i> , (2000)
red cell plasma membrane		0.45	Evans and Waugh, (1997)

where κ_b and κ_G are bending rigidity and Gaussian bending rigidity, respectively. The mean curvature is used to obtain bending energy. The Gaussian term is the difference between the actual energy of the system and its bending energy. As two important examples, the energy of two shells in the spherical with radius R and cylindrical with radius R and length L shapes compared to a flat surface can be written as follows [4].

$$\begin{aligned}
 E &= 4\pi (2\kappa_b + \kappa_G) \quad \textit{sphere} \\
 E &= \pi\kappa_b L/R \quad \textit{cylinder}
 \end{aligned}
 \tag{1.15}$$

Bending rigidity for selected lipid bilayers and cell membranes are presented in Table 1.3.

Some of the physical and mechanical properties of biomembranes presented in this section. In addition to these properties, there are some physical phenomenon such as buckling, which is the concern of this project, investigated during the last decades because of their importance. Buckling phenomenon and some of the scientific papers published about this

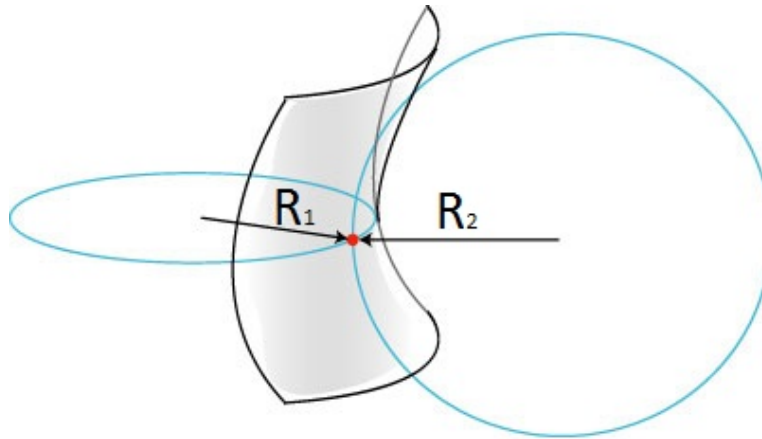


Figure 1.6: Schematic representation of a surface with nonzero curvatures.

specific phenomenon in biological membranes are explained later. Before, going to describe them, some mechanical modeling and analysis of whole cells are presented. Although the computer technologies have been developed during the last decades, modeling and simulation of cells including all of their organelles separately is not possible. The complexity of this small unit is much higher than what we can imagine. Hence, the cell models have been presented to model them as a whole. The compartments and organelles of the cell body have been simulated or modeled as single systems like the analysis of the bilayer membranes.

1.5 Cell mechanics

During the last decades, many scientists and engineers have investigated the mechanical properties of different organs, tissues and cells in order to obtain sufficient results for characterizing their behavior. By developing several techniques and instruments they started to investigate micro scale components and their properties in addition to the macroscopic ones. The cell as the building block of higher organisms took much more attention and causes to develop a new interdisciplinary field named Cellular Mechanics.

Table 1.3: Bending rigidity for selected lipid bilayers and cell membranes [4].

Membrane	$\kappa_b (\times 10^{-19})$	$(k_B T)$	Reference
diAPC	0.44 ± 0.05	11	Evans and Rawicz, (1990)
diGDG	0.44 ± 0.03	11	Evans and Rawicz, (1990)
	$0.15 - 0.4$		Duwe <i>et al.</i> , (1990)
	0.2 ± 0.07	5	Mutz and Helfrich, (1990)
diMPC	0.56 ± 0.06	14	Evans and Rawicz, (1990)
	1.15 ± 0.15	29	Duwe <i>et al.</i> , (1990)
diMPE	0.7 ± 0.1	18	Mutz and Helfrich, (1990)
diOPC	0.85 ± 0.10	23	Evans and Rawicz, (1990)
SOPC	0.90 ± 0.06	23	Evans and Rawicz, (1990)
red blood cell	$0.13 - 0.3$	$3 - 8$	Brochard and Lennon, (1975)
plasma	1.3	32	Evans, (1983)
membrane	$0.3 - 0.7$	$8 - 18$	Duwe <i>et al.</i> , (1990)
	$1.4 - 4.3$	$35 - 108$	Peterson <i>et al.</i> , (1992)
	0.2 ± 0.05	5	Zilker <i>et al.</i> , (1992)

Different mechanical properties of each cell can be affected by various factors such as existence of different kinds of external loads as well as diseases. In particular, cancer is a disease can greatly influences cell mechanical properties [72]. As an example, cancer cells are known to be 70 percent more compliant than benign cells. Recent studies of metastasis have shown the significance of the mechanical properties involved in carcinogenesis [65]. Alterations in cellular deformability, observed at the single cell level, have been already identified as a useful indicator of cancer-related changes [38]. Therefore, there is not still a thoroughly acceptable mechanical model to characterize the behavior of cells even a specific kind of cells in every condition though there are several articles and defined projects in this area.

The complexity of the structure of the cells cause they show nonlinear response to the

external loads. In addition, adaptation of behavior of cells in different conditions results in many problems for proposing a general model to characterize the mechanical behavior of the cells. Two fundamentally different approaches have been explored: the up-bottom approach in which a global model is proposed that reproduces some of the mechanical features of the cell, and the bottom-up approach in which individual components of the cell are modeled [70]. The first approach usually leads to continuum models, the second to discrete models.

In general, the domain of solution includes both the cell(s) and an outer medium (suspending fluid and ECM) which bears the outer boundary conditions. Different kinds of surface forces are applied on the cells. Surface tension forces and elasticity used in some models [27] have been accounted for forces applied by the outer part of the cytoskeleton, close to the actual membrane. Interaction forces between the adhesion molecules are the second kind of surface forces which coat the membrane and the cell environment. These forces can be investigated using different equations and models such as stochastic binding equations [34], kinetic equations [10] and averaged models, such as Van der Waals-type adhesion potentials [64]. Cells mostly exhibit a viscoelastic behavior. Strongly cross-linked structure of cytoskeleton determines the elastic part. The dissipating component giving rise to viscous-like behaviors has a contribution from the flow of the cytosol along with and through the cytoskeleton mesh-work. Rearrangement of cytoskeleton is another source of dissipation whose cross-links have a lifetime of the order of 1 second [63].

1.5.1 Viscoelastic models of red blood cell

Adult humans have roughly 20–30 trillions red blood cells at any given time, comprising approximately one quarter of the total human body cell number. RBCs contain hemoglobin, an iron-containing protein, which facilitate transportation of oxygen by reversibly binding to this respiratory gas and greatly increasing its solubility in blood. Number of these cells and their important roles in our body caused establish several studies about different mechanical properties of red blood cells in different conditions, the methods of measurements

of these properties and the effects of external stimuli on the cells.

Theoretical models, which attempted to describe dynamic behavior of RBC, indicate such behavior depends on membrane elastic properties, shear rate, and viscosities of the membrane and internal/external fluids. RBC dynamics in capillary flow is characterized by a transition from biconcave to parachute shapes as the flow rate is increased. The transition appears to be governed by the RBC membrane elastic and bending properties, as found in [48]. To capture realistic behavior of RBCs, mechanical models have to include:

- Membrane viscoelasticity with a viscous contribution of the lipid bilayer and with an elastic contribution of the spectrin network;
- Membrane bending resistance;
- Separate external/internal fluids with distinct viscosities.

In this section, some of the articles focused on mechanical properties of RBCs are presented to show progress of technologies and mathematical models for this purpose.

Rand [56] used an approach called micropipette aspiration to characterize RBCs. In this technique, the stress required to rupture the red cell membrane could be measured. He showed that the membrane can withstand a wide variety of tensions, up to a maximum of 20 dynes/m for short periods of time. He presented a temporal relation for tension in the membrane and finally proposed the following equation as viscoelastic model for the cells (Fig.(1.7))

$$S = F \left[\frac{1}{Y_2} + \frac{1}{Y_1} \left(1 - \exp \left(-\frac{Y_1}{\eta_1} t \right) \right) + \frac{1}{\eta_2} t \right] \quad (1.16)$$

One of the unique properties of red blood cells is its biconcave shape. Canham [6] explained this special shape using the minimum energy of bending. On the basis of the bending relation (based on the curvature of the surface ignoring other membrane forces), the energy was determined for many surfaces of revolution having the same area and volume. The geometry and energy of the shape with least energy closely approximated the bending energy and geometry of the actual red-cell profile with same area and volume.

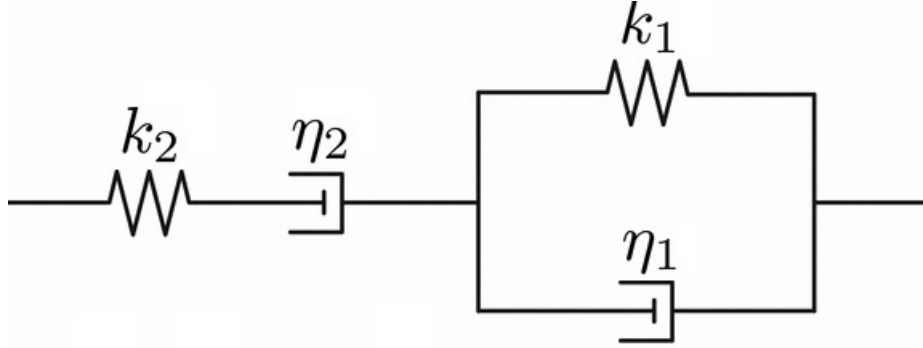


Figure 1.7: Mechanical model of the cell membrane used to describe the kinetics of the membrane breakdown [56]; k_1 and k_2 are two springs and η_1 and η_2 are two dashpots in the schematic model.

Jay (1973) [31] added some new information about the behavior of red blood cells in micropipette aspiration test and the limitations of this kind of testing. He investigated the conditions in which the shapes of the cells are reversible. Jay showed that human red cells can be drawn into cylindrical glass micropipettes of internal diameter approximately $2.0\mu\text{m}$.

Jay and Canham presented another article at 1977 [32] together about the micropipette aspiration of RBC. Measurements were made from 16mm film records that allowed the determination of the cellular area and volume of the individual erythrocyte as they were drawn into a $2.0\mu\text{m}$ pipette with negative pressure. Tozeren *et al.* [8] investigated dynamic rheological properties of the cell membrane employing micropipette aspiration. They illustrated that the rheological properties of the membrane can undergo dynamic changes depending on the extent and duration of deformation, reflecting molecular rearrangement in response to membrane strain. They used a generalization of Kelvin model (Evans and Hochmuth [29]) to present the following viscoelastic stress-strain relation of the RBC membrane

$$T_{ij} = -p\delta_{ij} + 2\mu\epsilon_{ij} + 2\eta v_{ij} \quad (1.17)$$

where T_{ij} is membrane tension, $(-p)$ is the pressure term due to constant surface area, μ is the coefficient of elasticity, η is the coefficient of viscosity, and V_{ij} is the components of the rate of strain tensor.

A nonlinear viscoelastic relation was developed by Chien *et al.* [69] to describe the viscoelastic properties of erythrocyte membrane. The presented constitutive equation used in the analysis of the time-dependent aspiration of an erythrocyte membrane into a micropipette. The inverse problem of obtaining the time dependency of the aspiration length from a given relaxation function was also solved. Analytical results obtained were applied to the experimental data of Chien *et al.* [8].

Suresh *et al.* [41] presented new experimental and computational results on shape evolution, force-extension curves, elastic properties and viscoelastic response of human red blood cells subjected to large elastic deformation using optical tweezers. They used different mathematical models and verified them with experimental results. Following equations were used in their modeling of cell membrane as incompressible solid [15, 16]

$$\begin{aligned} T_s &= 2\mu\gamma_s = \frac{\mu}{2} (\lambda_1^2 - \lambda_2^2) \\ T_s &= \frac{1}{2} (T_1 - T_2) \text{ and } \gamma_s = \frac{1}{2} (\epsilon_1 - \epsilon_2) = \frac{1}{2} (\lambda_1^2 - \lambda_2^2) \\ \lambda_1\lambda_2 &= 1 \end{aligned} \tag{1.18}$$

where T_1 and T_2 are the in-plane principle membrane stresses, ϵ_1 and ϵ_2 are the in-plane principle Green's strains of the membrane, μ is the membrane shear modulus and γ_s is the shear strain. The assumption of a constant area for the cell membrane is usually invoked, as indicated in third relation of Eq.(1.18). They also used the formulation of strain energy potential function presneted by Yeoh[75], which proposed as a modified one parameter Neo-Hookean model (a hyperelastic model), as follows

$$U = \frac{G_0}{2} (\lambda_1^2 + \lambda_2^2 + \lambda_3^2 - 3) + C_3 (\lambda_1^2 + \lambda_2^2 + \lambda_3^2 - 3)^3 \tag{1.19}$$

where the assumption of incompressibility was also taken into consideration. Here, G_0 is the initial value of bulk shear modulus, and λ_i (1 – 3) are the principle stretches. The incompressibility condition implies that $\lambda_1\lambda_2\lambda_3 = 1$.

The value of the parameter C_3 chose to be $G_0/30$ which best matched the experimental data. Three-dimensional computational simulations of the loading response were also performed by incorporating the viscoelastic term to the constitutive behavior of the cell membrane by modifying Eq.(1.18) [9, 28] as

$$T_s = \frac{\mu}{2} (\lambda_1^2 - \lambda_1^{-2}) + 2\eta \frac{\partial \ln \lambda_1}{\partial t} \quad (1.20)$$

where η is the coefficient of surface viscosity of the cell membrane, and μ is the in-plane shear modulus of the membrane.

The first measurements of the complex modulus of the isolated red blood cell presented by Turner *et al.* [55].

They computed elastic and frictional moduli g' and g'' using magnetic twisting filed. The cell took under sinusoidal load and they used the approach of Fredberg and Stamenovic [22] for sinusoidal analysis of a nonlinear system and defined the apparent complex elastic moduli g^* as

$$g^* = g' + g'' \quad (1.21)$$

where g' and g'' are the storage and loss moduli, respectively. The components of the complex modulus were determined from the limits of $T_s(t) - d(t)$ loop and the area, A, bounded by the loop representing the energy dissipation per cycle or hysteresis. The phase angle ϕ , stiffness g' , and loss modulus g'' then become

$$\begin{aligned}
\phi &= \sin^{-1} \left(\frac{4A}{\pi \Delta T_s \Delta d} \right) \\
g' &= \left(\frac{\Delta T_s}{\Delta d} \right) \cos \phi \\
g'' &= \left(\frac{\Delta T_s}{\Delta d} \right) \sin \phi = \frac{4A}{\pi \omega \Delta d^2}
\end{aligned} \tag{1.22}$$

Finally, mathematical modeling of cell rheology employing generalized Voight viscoelastic solid model used by Fisseha and Katiyar [20] is presented as the most common model for investigating the mechanical behavior of RBC. The generalization of an incompressible Voight viscoelastic solid model can be written as follows

$$T_{ij} = -p\delta_{ij} + T_{ij}^e + T_{ij}^v \tag{1.23}$$

where T_{ij}^e is the stress associated with an elastic component that can be expressed as a function of strain, and T_{ij}^v the stress associated with viscous fluid depend on rate of deformation, $-p\delta_{ij}$ is also the reaction stress due to incompressibility.

A general viscoelastic constitutive equation can be written using principle stresses. Hence, the extension ratios in Cartesian coordinate can be written as follows

$$\lambda_1 = \frac{dy_1}{dx_1} \text{ and } \lambda_2 = \frac{dy_2}{dx_2} \tag{1.24}$$

where dx_1 and dx_2 are initial lengths and dy_1 and dy_2 are current lengths. The Green's strain tensor for large deformation is defined by

$$e_{11} = \frac{1}{2} (\lambda_1^2 - 1), \quad e_{22} = \frac{1}{2} (\lambda_2^2 - 1), \quad e_{12} = e_{21} = 0 \tag{1.25}$$

Assuming the membrane is treated as 2D elastic continuum, the principal membrane tensions T_i are expressed as

$$T_i = \frac{1}{\lambda_1 \lambda_2} \lambda_i \frac{\partial W}{\partial \lambda_i} \quad (i = 1, 2) \tag{1.26}$$

The membrane also can be assumed to behave like a Neo-Hookean solid material. The Neo-Hookean model can be used to analyze nonlinear behavior of system under large deformation. Therefore, strain energy function for a 2D membrane is given by [3]

$$W = \frac{Gh}{2} \left(I_1 + 2 + \frac{1}{I_2 + 1} \right) \quad (1.27)$$

where G is the shear modulus of elasticity of the membrane and h is the thickness of the membrane. The two-dimensional strain invariant I_1 and I_2 defined by Skalak *et al.* [61] as

$$I_1 = \lambda_1^2 + \lambda_2^2 - 2 \text{ and } I_2 = \lambda_1^2 \lambda_2^2 - 1 \quad (1.28)$$

The tensions T_1 and T_2 along the principle directions can be found as

$$\begin{aligned} T_1 &= \frac{Gh}{\lambda_1 \lambda_2} \left(\lambda_1^2 - \frac{1}{(\lambda_1 \lambda_2)^2} \right) \\ T_2 &= \frac{Gh}{\lambda_1 \lambda_2} \left(\lambda_2^2 - \frac{1}{(\lambda_1 \lambda_2)^2} \right) \end{aligned} \quad (1.29)$$

The procedure is summarized and just the final equations are presented. Hence, we have

$$\begin{aligned} T_{11} &= -p + \frac{Gh}{\lambda_1 \lambda_2} \left(\lambda_1^2 - \frac{1}{(\lambda_1 \lambda_2)^2} \right) + \frac{2\eta_m}{\lambda_1} \frac{d\lambda_1}{dt} \\ T_{22} &= -p + \frac{Gh}{\lambda_1 \lambda_2} \left(\lambda_2^2 - \frac{1}{(\lambda_1 \lambda_2)^2} \right) + \frac{2\eta_m}{\lambda_2} \frac{d\lambda_1}{dt} \end{aligned} \quad (1.30)$$

In the case of uniaxial tension, T_{22} would be equal to zero and the other component can be obtained as follows

$$\begin{aligned} T_{11} &= -\frac{Gh}{\lambda_1 \lambda_2} \left(\lambda_2^2 - \frac{1}{(\lambda_1 \lambda_2)^2} \right) - \frac{2\eta_m}{\lambda_2} \frac{d\lambda_1}{dt} \\ &+ \frac{Gh}{\lambda_1 \lambda_2} \left(\lambda_1^2 - \frac{1}{(\lambda_1 \lambda_2)^2} \right) + \frac{2\eta_m}{\lambda_1} \frac{d\lambda_1}{dt} \end{aligned} \quad (1.31)$$

During experience of the in-plane membrane deformation, the membrane area is constraint, that is $\lambda_1\lambda_2 = 1$ ($\lambda_3 = 1$), in this condition the in-plane shear modulus $\mu = Gh$ throughout the entire deformation [26]. Therefore, the following equation can be obtained

$$T_{11} = \mu \left(\lambda_1^2 - \frac{1}{\lambda_1^2} \right) + \frac{4\eta_m}{\lambda_1} \frac{d\lambda_1}{dt} \quad (1.32)$$

where μ is the membrane shear elastic modulus and η_m is the membrane viscosity. The values of these parameters for RBC membrane is presented in Table 1.4.

Table 1.4: Given and estimated values of the two parameters and rate of strain for RBC.

Parameter	Given value	Reference	Estimated values
Shear elastic modulus μ	0.01dyn/cm	[61]	0.012, 0.023dyn/cm
Membrane viscosity η_m	0.001dyn.s/cm	[61]	0.0015, 0.0025dyn.s/cm
Rate of strain ($D\lambda_1$)	$0.3s^{-1}$	[41]	0.2, $0.01s^{-1}$

1.6 Membrane analysis

In addition to the experiments done during the last decades, several theoretical and computational models developed to analyze mechanical behavior of membrane. As one of the initial efforts, Helfrich (1973) developed a mathematical modeling of membrane using Hamiltonian (energy-based) method. He proposed the elasticity theory for the lipid bilayers. In his article, it was discussed that the curvature elasticity is the only one can control nonspherical shapes of the system. These theoretical and analytical investigations have been continued presented later in this section. By developing computer technology and computational techniques, different approach based on the simulation of the system have been used to simulate the membranes. Atomistic molecular dynamics (MD) and coarse-grained methods have been employed to model the systems. Although atomistic simulations are more accurate, coarse-grained method can be used to simulate larger structures

because they run faster than atomistic MD. Therefore, it can be concluded that two different approaches have been used including theoretical and mathematical modelings and simulations to investigate behavior and properties of the membranes. Brief explanations about some of these articles are presented in this section.

1.6.1 Simulation

Since 1950s, simulations have developed grown by developing algorithms, computational methods and computer technologies [11]. If we consider two aspects of Science including observation and comprehension, the importance of simulation can be understood. Simulations can be play an important role to validate theories. In addition to experiments as traditional methods of observation, simulation can be considered as computer experiments to prepare results when an experimental probe is out of reach [11]. Simulations can be predictive and lots of phenomena have been predicted based on simulations. Simulations are the thord paradigm of research together with theory and experiments. These techniques can be employed as a comprehensive tools instead of theories. In some problems, obtaining an analytical or mathematical modeling is not possible and simulations can be used to prepare accurate results to be compared with experimental ones resulting in comprehension of the experiments. Here, some of the articles used the simulation techniques to investigate the mechanical and physical behavior and characteristics of membranes are presented.

Meshless model which is based on particle-based method have been used in several studies [59, 50, 49]. Shiba and Noguchi [59] employed two types of meshless membrane models based on the different curvature potentials. Meshless membrane model was used which posses only translational degrees of freedom and form quasi-two-dimensional structure. The meshless spin membrane model was also employed in which orientational degrees of freedom are also taken into consideration. The modeled membrane were simulated with Brownian dynamics in NVT ensembles (constant number of molecules N , volume V , and temperature T) [59, 50, 47]. The Monte Carlo (MC) simulations have been also employed

in some articles [49]. Coarse-grained model were used several times for large-scale simulations of membrane and sheets [47, 71]. The schematic representation of the model used by Vliegenthart [71] is shown in Fig.(1.8). In addition, coarse-grained simulations have been compared with analytical and atomistic MD simulations by Deserno *et al.* [30]. Different mechanical and physical properties of membranes and sheets have been also investigated using simulations. Shiba and Noguchi [59] used spin membrane model to estimate spontaneous curvature C_0 and the bending rigidity κ . In addition, they estimated C_0 based on the shape of the membrane strip by employing second-order moving least squares fit [49]. The estimation is also done in the work of Otter [51]. The elastic modulus and area compressibility was investigated in the paper and the effects of undulations on system size was taken into consideration.

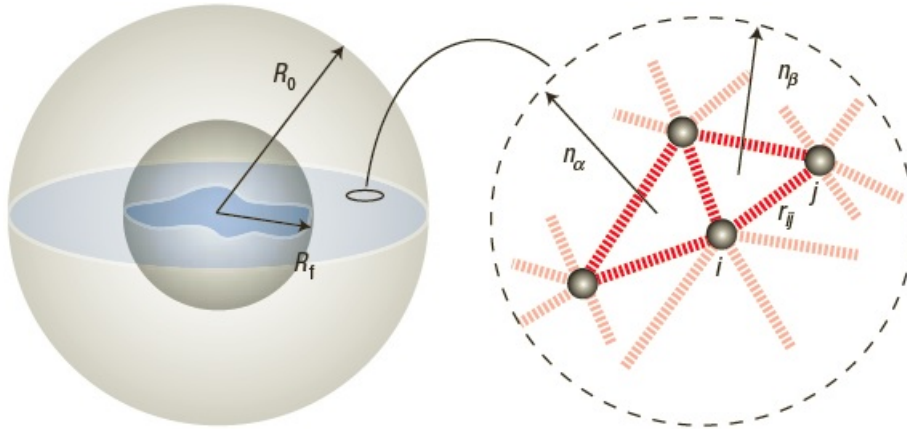


Figure 1.8: Schematic representation of the computer experiments (The picture is taken from [71]. Reproduced with permission from Nature). Left: By applying a force \mathbf{F} normal to the surface of the sphere its radius decreases from R_0 to its final radius R_f . Right: Microscopic detail of the triangulated surface model of a two-dimensional sheet (The details are available in [71]).

Different results about stress-strain relation and diagrams are available [51] can be used to obtain different variables in the system. The equilibrium areas per amphiphilic calculated as the roots of polynomials fitted through the stress-strain data [51]. Proper-

ties of fluid membranes were also investigated by Noguchi [47]. The surface tension of a flat membrane has been presented in his paper. Dependency of membrane properties on parameter values were investigated for a tensionless membrane. Membrane elasticity was also investigated by Noguchi and Gompper [49]. They studied equilibrium properties of self-assembled membrane such as bending rigidity, line and surface tensions.

Noguchi and Gompper [50] investigated formation of disklike micelles and vesicles. They concluded that the self-assembly consists of three process: (i) the particle assembly into discoidal clusters, (ii) the discoidal clusters aggregate into larger clusters, and (iii) the large disks close and form vesicles. They also observed that the average cluster size grows faster than what is observed in simulation when there is hydrodynamic interaction. It not only affects the time scale but also the membrane shape during closure. Noguchi investigated self-assembly of lipids in another paper [47]. The differences between the procedure and the conditions of forming droplets and vesicles were described.

As important phenomena in biomembranes, buckling and crumpling of the membranes have been investigated several times in different conditions and for different applications [46, 30, 71, 24, 51]. The buckled monolayer membrane is illustrated in Fig.(1.9) to show the discussed phenomenon. Because of small ratio of membrane thickness to its other dimensions, which is one of the primary geometrical properties of membrane, buckling and crumpling are among the important phenomena have been considered several times [51, 71]. In addition, there are different variables parameters such as surface tension which are some important in the considered environment and should be known in this phenomena. Buckling and collapse of lipid monolayer membranes were investigated [2]. Moreover, the collapse of the monolayer membrane initiated by buckling was shown. It was also shown that buckling of monolayers followed by their folding into bilayers to release the stress of bending deformation. The possibility of vesicle formation by transforming bilayer folds in the energetic point of view and the macroscopic properties affect this procedure was investigated in the paper. Otter [51] investigated the buckling phenomenon in lipid bilayers with neglecting undulations. The effects of thermal undulations and fluctuations have been also investigated [59, 49]. In addition, the transient behavior of the membranes

investigated about buckling phenomenon [24].

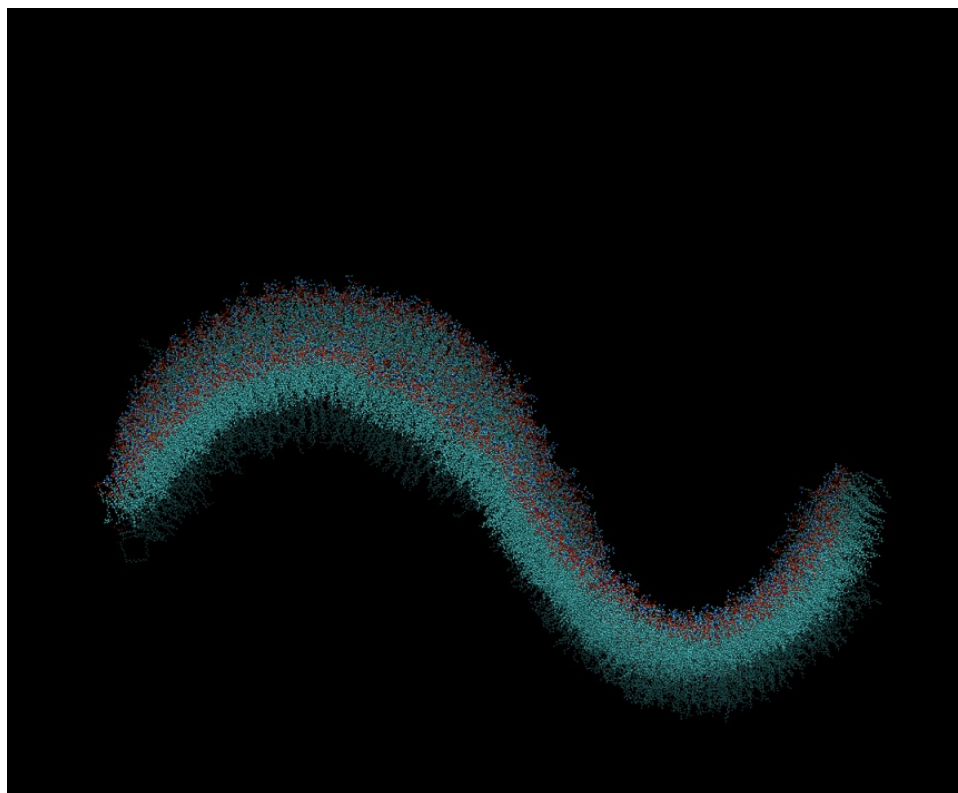


Figure 1.9: Buckled monolayer membrane using atomic simulation (Figure courtesy of Bin Liu, SoftSimu Group, University of Waterloo.).

1.6.2 Analytical investigations

The analytical modeling of lipid biomembranes using elasticity theory was proposed by Helfrich [25] in 1973. He used elasticity theory to define Hamiltonian and energy function to obtain an analytical modeling of the membrane. Nonlinear elasticity and stress functions were used to develop the model. It was shown that curvature is the only elasticity controlling nonspherical shape for closed bilayer films. The stresses in a closed lipid

membrane were investigated employing Helfrich Hamiltonian [7]. They investigated the response of the Hamiltonian to surface deformations. They considered the case of a surface dominated by surface tension in a soap bubble to illustrate their ideas. Rotations and torque were also taken into consideration. In addition, they showed that their model is well-established particularly when the membrane geometry possesses some degree of spatial symmetry. Domokos *et al.* [12] also investigated uplifted heavy elastic strip using Hamiltonian in the global equilibrium condition. The model can be used to the membranes based on the similar geometries. They used dimensionless variables to generalize the both the model and the obtained results. Moreover, the breaking of the symmetry of the system was investigated in details.

The Hamiltonians and energy functions used to obtain the final modeling of the system resulted in elliptic functions in some articles such as the work of Noguchi [46] also used to verify some of the results of the project for in-equilibrium membrane profiles under buckling. In addition, some of the functions has been solved using perturbation theory by Witten *et al* [77]. The mechanical buckling instabilities of a rigid film was investigated. As an example, the large deformations of the system can be obtained using expansion of the equations based on small deformation in perturbation analysis.

Several analytical studies have been dedicated to investigate buckling phenomenon [46, 30, 42, 53]. Noguchi [46] investigated anisotropic surface tension of buckled lipid membranes. The energy function of the monolayer membrane in one-dimensional approximation was derived based on the bending of the membrane. It was assumed that the length of the buckled membrane is constant as a criteria in the model. Noguchi used the derived elliptic functions as the solution of the membrane profile to obtain the surface tension in the monolayer membrane. In addition, interaction of between buckled membrane in a system include multiple membranes was investigated in his paper. Buckling of Langmuir monolayer was also investigated [42]. It was shown that a surfactant monolayer may have a instability similar to the buckling instability of a beam in one-dimension or a plate in two-dimensions if it goes under compression. Deserno *et al.* [30] presented an analytical solution of buckling of the lipid membrane. The elliptic functions were employed to ob-

tain the solution and the membrane profile after buckling. The solutions also obtained in the presence of undulations in the system. It was shown that the fluctuations result in shrinkage of the membrane and affect the membrane profile and other results presented in the paper [30]. Buckling transitions were investigated in spherical shells by Nelson *et al.* [39]. They used the model to characterize the virus shape and its behavior in the considered conditions. Topological defects on the curved surfaces were also studied as an important parameter in the problem. The spherical membranes were also modeled by Chen *et al.* [76]. The modeled system (core/shell structure) was solved employing finite element method (FEM). The undulating topology also was taken into consideration. The modeled membrane can be used as promising model of natural fruits in the considered conditions. Zhang and Witten [77] studied supported monolayer on a fluid film. The problem was solved to obtain the behavior of the considered membrane in buckling phenomenon. They also investigated fluctuations in the membrane and second-order buckling transition. Fluctuations and Goldstone modes (Fig.(1.10)) of fluid membrane tubules were studied by Fournier and Galatola [21]. The Goldstone mode can be defined as a long-wavelength fluctuation of the corresponding order parameter which breaks the symmetry of the system. It can also be defined as low energy excitation. If the microscopic Hamiltonian has full rotational symmetry, we expect that a uniform rotation costs no energy and as rotation which is slowly varying in space to cost very little energy.

There are some other articles solved buckling and large deformation of beams and membranes using other methods and numerical procedures [33, 23, 74]. There are some papers solved the buckling phenomenon using FEM packages such as Abaqus [33]. Taheri *et al.* [33] solved the dynamic plastic buckling of a slender beam. They considered that axial impact load applies to the beam. The dynamic buckling criterion was also studied in the paper. Sensitivity analysis can be so useful

to consider the effects of different parameters and conditions on the system was done by Taheri *et al.* [33]. Moreover, dynamic pulse buckling of composite shells investigated by Fatt *et al.* [23] They considered the shells to be under external blast. The effects of different parameters on dynamic behavior of the problem was also studied. As a different

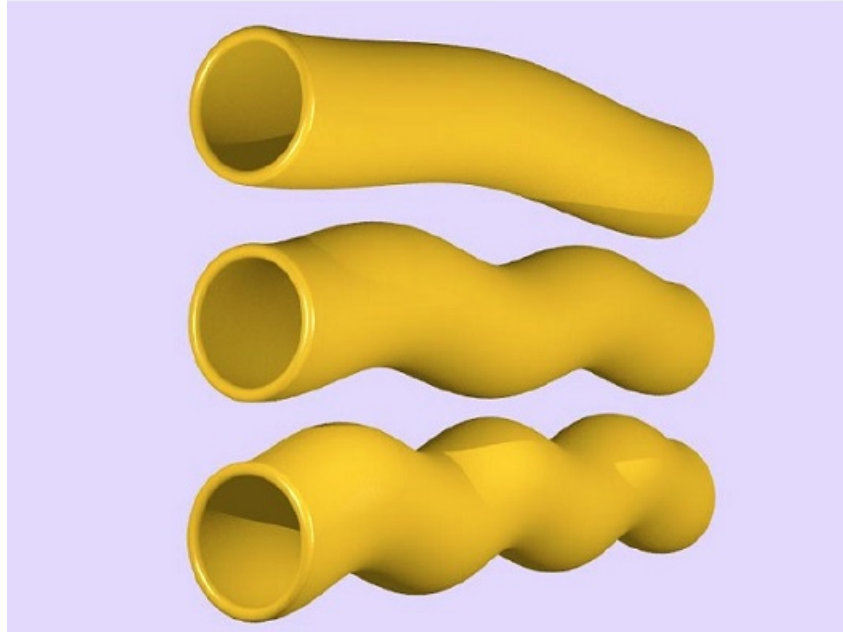


Figure 1.10: Goldstone modes ($m = 1$). From top to bottom $n = 1$, $n = 2$ and $n = 3$. (The picture is taken from [21]. Reproduced with permission from American Physical Society).

approach, the dynamic large deflection of a cantilever beam was studied using dynamic of infinitesimal elements of the whole beam by Xiet *al.*[74]. The model was solved using finite difference method and verified by the results of Abaqus as a FEM package.

In the next section the mathematical and numerical procedure used to solve different problems, statics and dynamics of monolayer membrane and static analysis of bilayer membrane, of this project are presented.

Chapter 2

Methods

In this section, mathematical models and numerical approaches used to solve different problems investigated in this projects are presented. The models are based on elasticity of the systems. The continuum equations of the problems are obtained and using equilibrium or dynamics of the infinitesimal elements. In order to solve the obtained highly nonlinear differential equations, finite difference schemes are employed. The details of the mathematical and numerical procedures are described in this section.

2.1 Mathematical modeling

Static and dynamic analysis of large deflection of thin heterogeneous membranes are obtained to be able to investigate transient and in equilibrium behavior of the buckling phenomena in biomembranes. The large deflection theory has been used and some new formulas are presented to be able to obtain the results of the problems for both small and large deformations. It should be noted that all of the equations are changed to the non-dimensional forms as more general formulas can be used to investigate different systems. The general formulas presented in this section help us to obtain the results of both homogeneous and heterogeneous membranes. Therefore, these general models can be used

to illustrate the effects of different parameters such as stiffness of the membrane on its buckling and its large deformation behavior.

2.1.1 Static analysis of membrane

One-dimensional buckling analysis of the thin membrane is modeled using straight Euler-Bernoulli beam in this article. The presented model is considered to be general to be able to employ it in the large deflection analysis. Buckling of the membrane can be considered as a large deflection problem not a small one. It is based on the existence of large deformation and curvature in the membrane.

In this section, equilibrium equations of large deflection of a one-dimensional thin membrane is presented. Some of the important geometrical and physical properties of the considered membrane are presented in Fig.(2.1). It should be noted that the presented model for static analysis of monolayer membrane is based on the modeling part of the work done by Maleki *et al* [40]. In this figure, length of the the considered element ds , the curvature of the element R , Horizontal and vertical forces F_x and F_y , bending moment M and slope of the membrane at the considered position $\theta(s)$ are clearly shown. In addition, following geometrical relations can be used to obtain the system of equations of the problem

$$\begin{aligned} dx &= ds \cos(\theta) \\ dy &= ds \sin(\theta) \end{aligned} \tag{2.1}$$

where ds is the length of the element. Two dimensional equilibrium equations of the membrane can be written as follows in order to obtain suitable relations between the momentum M and the internal forces

$$\begin{aligned} \sum F_x = 0 &\Rightarrow \frac{dF_x}{ds} = 0 \Rightarrow F_x = cte. \\ \sum F_y = 0 &\Rightarrow \frac{dF_y}{ds} + \omega(s) = 0 \Rightarrow F_y = - \left(\int \omega(s)ds - \int \omega(s)ds|_{s=L} \right) \\ \sum M = 0 &\Rightarrow \frac{dM}{ds} = F_y \cos \theta + F_x \sin \theta \end{aligned} \tag{2.2}$$

where M is the internal bending moment and F_x and F_y are horizontal and vertical internal forces, respectively. In addition, the constitutive equation of Euler-Bernoulli beam can be written as follows

$$\frac{M}{EI} = \frac{1}{R} = \frac{d\theta}{ds} \Rightarrow M = EI \frac{d\theta}{ds} \quad (2.3)$$

as the fourth equation required to solve the obtained system of equations.

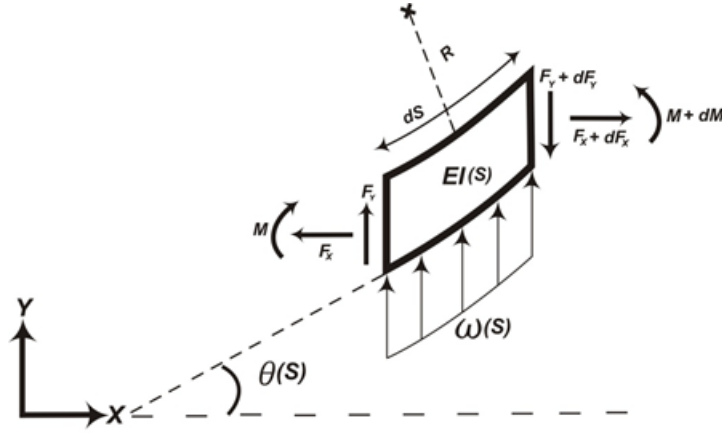


Figure 2.1: A schematic model of an element of the membrane.

Therefore, the following nonlinear differential equation can be obtained using Eqs.(2.2) and (2.3).

$$\frac{d}{ds} \left[EI \frac{d\theta}{ds} \right] + \cos \theta \left(\int \omega(s) ds - \int \omega(s) ds |_{s=L} \right) - F_x \sin \theta = 0 \quad (2.4)$$

In order to have a general solution, it is necessary to rewrite Eq.(2.4) in the non-dimensional form as follows

$$\frac{d}{ds^*} \left[\lambda(s^*) \frac{d\theta^*}{ds^*} \right] + \cos \theta^* \left(\int \omega^*(s^*) ds - \int \omega^*(s^*) ds^* |_{s^*=1} \right) - F_x^* \sin \theta^* = 0 \quad (2.5)$$

which is obtained using the following non-dimensional parameters

$$s^* = \frac{s}{L}; \quad \omega^*(s^*) = \frac{\omega(s)}{\omega_{\max}}; \quad \lambda(s^*) = \frac{EI(s)}{\omega_{\max} L^3}; \quad F_x^* = \frac{F_x}{\omega_{\max} L} \quad (2.6)$$

where L is the half length of the membrane and ω_{max} is the maximum amount of distributed load applied on it.

In order to obtain the behavior of the homogeneous and heterogeneous membranes, Eq.(2.5) should be solved in the general form. The numerical procedure used to solve the problem is described in the next section.

In addition to the one-dimensional analysis of thin membrane, two dimensional analysis of the symmetric circular membrane is presented. In the case of one-dimensional membrane, the criteria of constant length equivalent to incompressibility of the membrane is used. In order to investigate circular membrane, because of considering two-dimensional behavior of the system, the criteria of constant area are used to obtain the solution. It is obvious that in the case of two dimensional problem in cylindrical coordinate which is our concern, we should have two equations in $r - z$ and $\phi - r$ planes. However, because of assuming the circular symmetry, all of the variables and parameters do not depend on ϕ . Therefore, the equation of the equilibrium of the symmetric circular membrane can be written same as Eq.(2.5) in the non-dimensional form with just one important modification. The modification is based on the criteria of constant area. Let us consider a circular membrane with radius L_0 . If we consider a point in the membrane in the distance R from the center, and this point goes to another position after buckling in distance r from the centerline, we will have the following relation as incompressibility equation

$$\frac{ds'}{ds} = \frac{R}{r} \quad (2.7)$$

where ds and ds' are the initial and final elemental lengths of the membrane at that position, respectively. In the Numerical procedure section, it is completely described that how we can use this relation to solve the equation with the considered criteria.

2.1.2 Static analysis of bilayer membrane

One of the important physical systems in the biological context is bilayer membrane as the covering of different cell type and their organelles such as mitochondria. They include two

layers (mostly constructed by lipids) each has similar behavior to monolayer membrane investigated in the previous part of this chapter. One thing causes the analysis of the bilayer membrane much more complicated than the monolayer one is the incompressibility of the bilayer membrane.

Although the static model for analysis of membrane is presented in the section 1.1.1, in the case of bilayer membrane some modifications are required based on the incompressibility restriction. If we use just the presented static model of monolayer membrane, by increasing the deflection of the membrane, the layers will come near or even go through each other. Therefore, some modifications should be considered to satisfy the constraint of incompressibility of the bilayer membrane. In molecular dynamic simulation, different forces and momentum should be considered to simulate the system. There are coulomb and van der Waals forces can be considered as two extensional forces, e.g. they apply forces along centerline of the considered particles. In addition, there is a momentum to hold the bond angles. With due attention to these forces and momentum in molecular dynamic simulation, the inspired bilayer model is presented in this section to be able to presented a promising method of analysis of bilayer membrane without the computational costs of MD simulations.

In order to apply the modifications, two springs are considered between the nodes of the discretized domain described in the next section (Fig.(2.2)). The presented extensional spring is a linear spring obeys Hook's law or linear stress-strain constitutive law $\sigma = E\epsilon$. On the other hand the considered bending spring is a nonlinear one which the following equation is considered as its constitutive law

$$M = |\delta\phi|^2 \delta\phi^{3/4} \quad (2.8)$$

Therefore, the bilayer membrane is modeled using the differential equation of the monolayer membrane (Eq.(2.5)) and solved for each layer. Moreover, the linear extension-compression and nonlinear bending springs are used in order to satisfy the incompressibility criteria of the bilayer membrane.

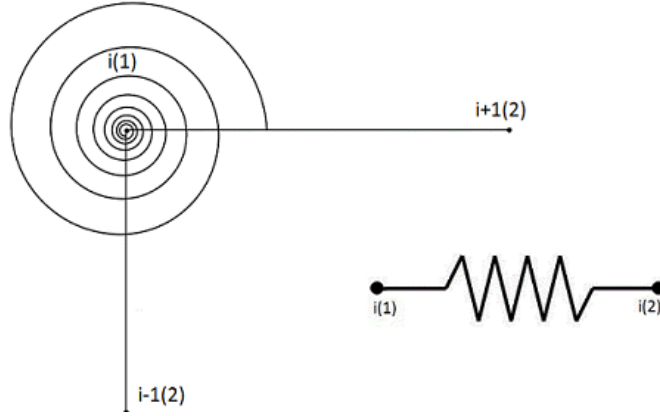


Figure 2.2: Schematic models of the springs considered between the nodes of the layers of the bilayer membrane (1 and 2 represent the first and second layers and i is the node number).

2.1.3 Dynamic analysis of membrane

In order to model the transient buckling behavior of half thin membrane, the equations of the previous part should be changed to include acceleration terms. Therefore, Fig.(2.1) can be considered also as free body diagram of the dynamic problem. The geometrical equations (Eq.(2.1)) is still true and the equilibrium equations (Eq.(2.9)) should be changed to the following equations of motion of the membrane.

$$\begin{aligned}
 \sum F_x = ma_x &\Rightarrow \frac{\partial F_x}{\partial s} = \rho \frac{\partial^2 x}{\partial t^2} \\
 \sum F_y = ma_y &\Rightarrow -\frac{\partial F_y}{\partial s} - \omega(s) = \rho \frac{\partial^2 y}{\partial t^2} \\
 \sum M = J\alpha - \rho ds \frac{\partial}{\partial t} \left(y \frac{\partial x}{\partial t} - x \frac{\partial y}{\partial t} \right) & \\
 \Rightarrow \frac{\partial M}{\partial s} - F_x \sin(\theta) - F_y \cos(\theta) = J\ddot{\theta} - \rho \frac{\partial}{\partial t} \left(y \frac{\partial x}{\partial t} - x \frac{\partial y}{\partial t} \right) & \quad (2.9)
 \end{aligned}$$

where ρ is linear mass density of the membrane, J is its moment of inertia and α is angular acceleration. The presented equations can be changed using the geometrical relations of

Eq.(2.1) to the following ones

$$\begin{aligned}
\frac{\partial F_x}{\partial s} &= \rho \frac{\partial^2}{\partial t^2} \int \cos(\theta) ds \\
-\frac{\partial F_y}{\partial s} - \omega(s) &= \rho \frac{\partial^2}{\partial t^2} \int \sin(\theta) ds \\
\frac{\partial M}{\partial s} - F_x \sin(\theta) - F_y \cos(\theta) &= J\ddot{\theta} \\
-\rho \frac{\partial}{\partial t} \left(\int \sin(\theta) ds \frac{\partial}{\partial t} \int \cos(\theta) ds \right) \\
-\rho \frac{\partial}{\partial t} \left(\int \cos(\theta) ds \frac{\partial}{\partial t} \int \sin(\theta) ds \right)
\end{aligned} \tag{2.10}$$

Therefore, the equations of motion of the membrane after applying the temporal derivatives can be written as follows

$$\begin{aligned}
\frac{\partial F_x}{\partial s} &= \rho \int (-\ddot{\theta} \sin \theta - \dot{\theta}^2 \cos \theta) ds \\
-\frac{\partial F_y}{\partial s} - \omega(s) &= \rho \int (\ddot{\theta} \cos \theta - \dot{\theta}^2 \sin \theta) ds \\
\frac{\partial M}{\partial s} - F_x \sin(\theta) - F_y \cos(\theta) &= J\ddot{\theta} \\
-\rho \left(\int \sin(\theta) ds \int (-\ddot{\theta} \sin \theta - \dot{\theta}^2 \cos \theta) ds \right) \\
-\rho \left(\int \cos(\theta) ds \int (\ddot{\theta} \cos \theta - \dot{\theta}^2 \sin \theta) ds \right)
\end{aligned} \tag{2.11}$$

which can be changed to the following equations by taking derivative from both sides of the two first equations

$$\begin{aligned}
\frac{\partial^2 F_x}{\partial s^2} &= \rho \left(-\ddot{\theta} \sin \theta - \dot{\theta}^2 \cos \theta \right) \\
-\frac{\partial^2 F_y}{\partial s^2} - \frac{\partial \omega(s)}{\partial s} &= \rho \left(\ddot{\theta} \cos \theta - \dot{\theta}^2 \sin \theta \right) \\
\frac{\partial M}{\partial s} - F_x \sin(\theta) - F_y \cos(\theta) &= J\ddot{\theta} \\
-\rho \left(\int \sin(\theta) ds \int \left(-\ddot{\theta} \sin \theta - \dot{\theta}^2 \cos \theta \right) ds \right) & \\
-\rho \left(\int \cos(\theta) ds \int \left(\ddot{\theta} \cos \theta - \dot{\theta}^2 \sin \theta \right) ds \right) &
\end{aligned} \tag{2.12}$$

The obtained equation should be changed to the non-dimensional form to be able to generalize the solution for different materials and geometries. The non-dimensional forms of the Eq.(2.12) can be written as

$$\begin{aligned}
\frac{\partial^2 F_x}{\partial s^2} &= \rho^* \left(-\ddot{\theta} \sin \theta - \dot{\theta}^2 \cos \theta \right) \\
-\frac{\partial^2 F_y}{\partial s^2} - \frac{\partial \omega(s)}{\partial s} &= \rho^* \left(\ddot{\theta} \cos \theta - \dot{\theta}^2 \sin \theta \right) \\
\frac{\partial}{\partial s} \left(\lambda \frac{\partial \theta}{\partial s} \right) - F_x \sin(\theta) - F_y \cos(\theta) &= J^* \ddot{\theta} \\
-\rho^* \left(\int \sin(\theta) ds \int \left(-\ddot{\theta} \sin \theta - \dot{\theta}^2 \cos \theta \right) ds \right) & \\
-\rho^* \left(\int \cos(\theta) ds \int \left(\ddot{\theta} \cos \theta - \dot{\theta}^2 \sin \theta \right) ds \right) &
\end{aligned} \tag{2.13}$$

where $\rho^* = \rho L / \omega T^2$ and $J^* = J / \omega T^2 L$ are the dimensionless density and moment of inertia, respectively and all temporal derivatives are changed to the dimensionless form using T as the time necessary for system to be reached to the steady state. The obtained nonlinear integrodifferential equations of dynamic large deflection of membrane are solved employing finite difference schemes described in the next section.

After obtaining some results and comparing them with available ones in literature, it found

that the presented model need some modification. In the case of dynamic analysis, dissipation of the system should be considered in the presented model. In any natural or artificial system, there is energy dissipation affects the dynamic behavior of that system. These energy dissipations are taken into considerations as modifications of the presented model (Eq.(2.13)) so that a bending dissipation and transverse deflection dissipation terms are considered in the system. The bending dissipation is modeled using the bending damping C and the transverse deflection dissipation is modeled using the dimensionless parameter D . The considered bending dissipation affects the behavior of the system as $C\dot{\theta}$. It is considered as a dissipation force in the presented model. In addition, the transverse dissipation applies $D\dot{y}$ as another dissipation force. These forces cause the system grows smoothly from its initial state to the final one. This smoothness is different for every system which its value can be set as suitable one to properly models the dynamic behavior of that system.

Chapter 3

Numerical procedure

In order to obtain the solution of the different models presented in the previous section including static 1D and 2D static analysis of thin membrane and dynamic large deflection of one-dimensional membrane, the suitable finite difference scheme is used in each case. The employed approaches are described in this section to clarify the numerical procedure of the solution.

3.1 Static analysis of membrane

The obtained nonlinear differential equation of the problem (Eq.(2.5)) is solved using the finite difference scheme as described in this section. On the basis of steady state condition of the problem, iterative method is used to solve the obtained discretized equation (Eq.(3.1)) in a considered mesh-grid of the one-dimensional domain. The discretized form of the Eq.(2.5) can be written as follows

$$\frac{\lambda_{i+1}^{n+1} \frac{d\theta^{n+1}}{ds_{i+1}} - \lambda_{i-1}^{n+1} \frac{d\theta^{n+1}}{ds_{i-1}}}{2\delta s} + \cos \theta_i^n \left(\int \omega^*(s^*) ds - \int \omega^*(s^*) ds^*|_{s^*=1} \right)_i - F_x^* \sin \theta_i^n = 0 \quad (3.1)$$

where $d\theta/ds|_k^m$ is the second order central derivative of θ at node k and iteration m . In Eq.(3.1), δs represents grid size and i and n are node and iteration numbers, respectively. This equation can be rewritten as the following equation in the case of constant λ (homogeneous membrane)

$$\lambda \frac{\theta_{i+1}^{n+1} - 2\theta_i^{n+1} + \theta_{i-1}^{n+1}}{\delta s^2} + \cos \theta_i^n \left(\int \omega^*(s^*) ds - \int \omega^*(s^*) ds^*|_{s^*=1} \right)_i - F_x^* \sin \theta_i^n = 0 \quad (3.2)$$

The system of equations obtained using the discretized differential equation written at each node (Eq.(3.1)) can be written in the matrix form. The matrix form then is solve at each iteration. It should be noted that the obtained equations are based on the distributed vertical loads applied on the membrane. If we want to solve the problem for applied vertical concentrated load, the equations will be the same and just there will be a concentrated load in one point of the discretized domain.

Because of the symmetry of the considered domain, half of the membrane is solved using the wall boundary conditions $\theta = 0$ at the left side of the domain and middle of the membrane. In addition, it can be easily concluded that no boundary force in y -direction should be considered in the case of no external vertical load.

3.2 Static analysis of bilayer membrane

It is described in the modeling section that the differential equations of the monolayer membrane can be considered as in-equilibrium equations of each layer of the bilayer membrane. Therefore, the iterative procedure described for the numerical analysis of the static monolayer membrane problem can be also employed to solve this problem. It should just be noted that the presented modifications in the modeling part cause some differences in the procedure of obtaining the system of equations of the domain. As it is shown in Fig.(2.2), there are two springs attached to each node in every membrane. The extension-compression spring is considered between node i of the two layers. The bending spring is

also attached between node i of one layer and nodes $i - 1$ and $i + 1$ of the other one as shown in Fig.(2.2).

3.3 Dynamic analysis of membrane

In order to investigate time-dependent behavior of the membrane, system of nonlinear partial differential equations (Eq.(2.13)) should be solved using a suitable numerical approach. The time-dependent finite difference scheme is chosen to solve the problem. The approach is based on the implicit time-dependent FDM. In this approach, the equations are discretized as follows to obtain a discrete PDE including the variables at different nodes and time-stages so that the nonlinear PDEs change to a linear finite difference equation.

$$\begin{aligned}
& \left(\frac{\partial^2 F_x}{\partial s^2} \right)_i^{n+1} = \rho \left[-\ddot{\theta}_i^n \sin(\theta_i^n) - \frac{\theta_i^{n+1} - \theta_i^n}{\delta t} \dot{\theta}_i^n \cos(\theta_i^n) \right] \\
& - \left(\frac{\partial^2 F_y}{\partial s^2} \right)_i^{n+1} - \left(\frac{\partial \omega(s)}{\partial s} \right)_i^{n+1} = \rho \left[\ddot{\theta}_i^n \cos(\theta_i^n) - \frac{\theta_i^{n+1} - \theta_i^n}{\delta t} \dot{\theta}_i^n \sin(\theta_i^n) \right] \\
& \frac{\lambda_{i+1}^{n+1} \frac{\partial \theta^{n+1}}{\partial s_{i+1}} - \lambda_{i-1}^{n+1} \frac{\partial \theta^{n+1}}{\partial s_{i-1}}}{2\delta s} - F_x|_i^{n+1} \sin(\theta)|_i^n - F_y|_i^{n+1} \cos(\theta)|_i^n = \\
& - \rho \left(\int \sin(\theta_i^n) ds \int \left[-\ddot{\theta}_i^n \sin(\theta_i^n) - \frac{\theta_i^{n+1} - \theta_i^n}{\delta t} \dot{\theta}_i^n \cos(\theta_i^n) \right] ds \right) \\
& - \rho \left(\int \cos(\theta_i^n) ds \int \left[\ddot{\theta}_i^n \cos(\theta_i^n) - \frac{\theta_i^{n+1} - \theta_i^n}{\delta t} \dot{\theta}_i^n \sin(\theta_i^n) \right] ds \right)
\end{aligned} \tag{3.3}$$

where

$$\begin{aligned}
\ddot{\theta}_i^n &= \frac{\theta_i^{n+1} - 2\theta_i^n + \theta_i^{n-1}}{\delta t^2} \\
\left(\frac{\partial^2 F_x}{\partial s^2}\right)_i^{n+1} &= \frac{F_x|_{i+1}^{n+1} - 2F_x|_i^{n+1} + F_x|_{i-1}^{n+1}}{\delta s^2} \\
\left(\frac{\partial^2 F_y}{\partial s^2}\right)_i^{n+1} &= \frac{F_y|_{i+1}^{n+1} - 2F_y|_i^{n+1} + F_y|_{i-1}^{n+1}}{\delta s^2} \\
\left(\frac{\partial \omega(s)}{\partial s}\right)_i^{n+1} &= \frac{\omega_{i+1}^{n+1} - \omega_{i-1}^{n+1}}{2\delta s}
\end{aligned} \tag{3.4}$$

As it is mentioned, these equations are linearized form of the original nonlinear PDEs (Eq. (2.13)). The obtained equations for each node and time stage should be gather together to construct a system of equations can be written in the matrix form. The obtained matrix form of the discretized equations for the whole domain at time stage $n + 1$ can be solved to obtain the matrix of coefficients and vector of variables including θ at all nodes of the domain. Therefore, instead of solving a static equation iteratively like the one for equilibrium analysis of membrane, the equations are solved at time stages to obtain the time-dependency of the behavior of the membrane.

3.4 Convergence, grid-independence and verification of the solution

In order to ensure about trustfulness of our modeling and numerical procedure, it is necessary to investigate the convergence of the numerical solution as well as obtain a grid size in the grid-independent region of the solution. The convergence of the solution is shown in Fig.(4.1) for different values of applied loads using norm defined as

$$N_\infty = \max|\theta_N - \theta_{N-1}| \tag{3.5}$$

where N is the number of nodes used to obtain the solution in the considered domain. It is obviously shown that $N = 300$ is enough to be considered as iteration numbers in all cases.

The difference of maximum values of θ for two grid-sizes $\max(\theta_{Nx}) - \max(\theta_{Nx-1})$ in which Nx is the number of nodes is illustrated in Fig.(4.2). It is observed in this figure that this difference decreases by decreasing the grid-size. As $1/\delta x$ grows, the oscillations are damped and all diagrams presented for different applied loads converge to a minimum limit. The solution after this grid-size shown in Fig.(4.2) is grid-independent. Therefore, $1/\delta x = 450$ is chosen in all cases to ensure about the grid-independency of the solution. In the next section, effects of changing different parameters are investigated on the membrane profile, maximum deflection, etc.

Chapter 4

Results and discussion

In this section, the results of the different problems investigated in this project are presented. The illustrated results are investigated and different aspects of the diagrams are explained in details. The descriptions are organized similar to the order of the results to simplify the comparison of the results of the problems in different conditions and using different parameter values. Although the diagrams of the different problems are compared to each other because of their relation, the explanations are categorized based on the considered problem to help us presenting different aspects of the considered problems separately.

4.1 Static analysis of membrane

The grid-independency and convergence of the solution should be considered as the first steps of the procedure of the solution to be sure about the trustfulness of the considered numerical procedure, time intervals and iteration numbers. In Fig.(4.1), convergence of the solution is shown using the iteration number N . It is obvious that all of the solutions considered for different applied horizontal loads are converged for iteration numbers more than $N = 300$ chosen in the numerical procedure. In addition, it is illustrated that there is

pick in all of the diagrams which is based on the behavior of the buckling phenomena. In the buckling phenomena, there is a sudden change of the shape of the system cause these kinds of convergence behavior. It should be noted that the solution converges faster for lower load values. In addition to the convergence, the grid-independency of the solution for the considered membrane under different applied loads are illustrated in Fig.(4.2). It is shown that by decreasing the grid size which is equivalent to increasing $1/\delta x$ the considered variable decreases to reach a region can be considered as grid-independent. In this problem, $1/\delta x$ is chosen based on Fig.(4.2) to obtain the grid-independent results. It should be noted that the variation of the considered variable with respect to $1/\delta x$ is oscillatory and the amplitudes of the oscillations decreases by increasing the values of the variable. Moreover, the considered variable is less depends on the grid-size for smaller applied loads.

In addition to the grid-independency and convergence of the solution, the obtained solution should be verified using the available results in the literature [46]. It is based on the fact that in mathematical point of view, we can obtain a converged and grid-independent solution based on a false physical model or a model with some deficiencies. Hence, the results should be compared to the results obtained employing different models and methods in the literature. Therefore, buckling of the membranes with half lengths $L = 2/3$ and $L = 4/3$ are presented in Figs.(4.3) and (4.4), respectively. The profiles have two regions including two opposite curvatures and the slope is zero at the left boundary and middle of the membrane. The curvature of the diagrams of Fig.(4.4) is larger than the other ones because of the higher value of applied load in that case. The result are verified with results of Noguchi [46] which are based on the following equations of the buckled profiles of the membrane (the procedure of obtaining these equations are described in the mentioned reference)

$$\begin{aligned} x &= 2bE [am(s/b, k), k] - s \\ y &= 2kbcn(s/b, k) \end{aligned} \tag{4.1}$$

where $E(a, k)$, $am(a, k)$ and $cn(a, k)$ are the elliptic integral of the second kind, Jacobi amplitude and Jacobi elliptic function, respectively. In addition, s is the arc length and k

can be determined using the following equation

$$\frac{L}{4b} = K(k) \quad (4.2)$$

It is clearly shown that the profiles of the membranes obtained using continuum model of this project and energy method of Noguchi [46] are coincide with each other. Henceforth, the continuum model can be used to obtain different results and investigate different behaviors of the membrane.

In order to investigate the buckling behavior of the membrane, membrane profiles obtained based on the different applied loads have primary importance. These profiles, shown in Figs.(4.5) and (4.6), clarify the behavior of the membrane in this specific phenomenon. Effects of the applied loads on the membrane profiles of the membranes with half lengths $L = 2/3$ and $L = 4/3$ are presented in these figures. The range of the applied loads are different for the membranes with different lengths which is based on the both physical behavior and dimensionless parameters of the system. The deflection of the membrane and its curvature increases by increasing the value of the applied load which is clarified in these figures. In addition, it seems that dependency of the maximum deflection cannot be considered as linear and its variation decreases by increasing the applied load. In order to clarify this dependency, maximum deflection and slope of the membrane profile for a membrane with length $L = 1$ is shown in Fig.(4.7). On the basis of the presented diagrams, maximum slope reach in liner dependent region while maximum deflection goes to reach a maximum value. Therefore, maximum deflection has a limit which is based on the conditions of the system and criteria of constant length.

In addition to the presented result based on the homogeneous membrane with $\lambda = 1.0$, it has worth to present some results related to a heterogeneous membrane. We are capable of presenting such kinds of results because of the general model (Eq.(2.5)) presented in this project. In order to show the effects of heterogeneity on the buckling of the membrane, a small part with length $l_h = 1/5$ is considered with different stiffness λ in the membrane. As one of the important variables of the system, variations of the maximum deflections of the membrane with respect to the starting position of the heterogeneous parts are shown

in Figs.(4.8) and (4.9) for the two membranes with heterogeneous stiffness $\lambda_h = 0.5$ and $\lambda_h = 2.0$. The membranes are considered to be under different applied loads. It is obviously shown that this heterogeneity has important effects on the buckling of the membrane. It can be concluded using the diagrams of Figs.(4.8) and (4.9) that there is an extremum region in the diagrams located at $a = 0.4$ corresponding to the existence of the heterogeneous part in the middle of the half membrane. It is based on the fact that the critical region of the half membrane is located in its middle part. We are solved the equation of the system to obtain θ as the primary dependent variable of the system. Hence, if we control its maximum value, we can affect the buckling or any other large deflection phenomena in the most effective way. In the case of softer heterogeneous part shown in Fig.(4.8), existence of the heterogeneity cause increasing the maximum deflection of the membrane while it has opposite effect if the harder one is considered in the system (Fig.(4.9)). Moreover, to show the effect of the stiffness of the heterogeneous part on the maximum deflection of the membrane, this dependency is illustrated in Fig.(4.10) for the half membrane with $L = 1$ and under different applied buckling loads. It is shown that by increasing the applied load, effect of heterogeneity on the maximum deflection decreases.

One of the criteria of the membrane analysis is constant length in the one-dimensional case. This criteria causes some restrictions such as a limit for maximum deflection of the membrane which is clarified before. In order to have a more realistic result, another model is also presented which is based on the symmetric circular system membrane. In this case the criteria of constant length changes to constant area which is more comparable to the natural systems. The profiles of the membrane with two half lengths $L = 2/3$ and $L = 4/3$ are presented in Figs.(4.11) and (4.12), respectively. It is illustrated in theses figures that the deflection of the membrane increases by increasing the applied load. However, it is not similar to the behavior of the one-dimensional membrane. In this case, L_x decreases much less than the increased value of L_y . The differences of the behavior of the circular and one-dimensional membrane are clarified in Fig.(4.13). It is shown that increasing the applied load causes increasing the maximum deflection and slope while results in decreasing L_x . The most important difference of this system with the one-dimensional membrane

can be clarified by comparison of this diagrams and the ones presented in Fig.(4.7). By employing the circular model, the restriction of maximum deflection is omitted. In addition, it is shown that L_x decreases as a linear function of the applied compression. It should be noted that variation of L_y is faster than L_x resulting in increasing the length of the circular membrane in side-wise view. In addition to the results of the homogeneous circular membrane, effects of heterogeneity is investigated (Fig.(4.14)). It is based on existence of the heterogeneous part in the middle of the half membrane shown as the most effective position. It is shown in Fig.(4.14) that increasing the stiffness of this small part causes decreasing the maximum deflection and slope of the membrane. Variation of maximum deflection is faster than slope of the membrane which is based on their physical definitions. These variations are nonlinear and do not approach to any limit or linear part.

4.2 Static analysis of bilayer membrane

Bilayer membranes play an important role in the nature specifically as outer layer of the Eukaryotic cells and their organelles. One of the physical phenomenon should be investigated about this coverages is buckling. As it is described in the case of monolayer membrane, applying a horizontal load may cause buckling. In the molecular point of view, this forces are based on the concentration of energy in a specific area. In other words, the molecules exist in a region prefer to buckle to minimize the energy of the system.

In order to show the buckling phenomenon in the bilayer membrane, the membrane profiles after buckling are presented in Figs.(4.15) and (4.16). In these figures, the profiles are shown for two different buckling loads applied to the same bilayer membrane resulting in different profiles. The profile of the Fig.(4.15) is based on $P_x = 41$ which is less than the applied load related to profile of Fig.(4.16). Hence, the deflections of the layers of the membrane in the case of Fig.(4.15) are smaller than the other one. It should be noted that because of the considered modifications with respect to the monolayer model, the deflection of each layer is different from deflection of the monolayer membrane with same

properties and under the equal buckling load.

The model of the monolayer membrane is modified to be used in analysis of bilayer membranes. Because of the importance of the bilayer membranes in micro scale, the modification is applied based on the molecular point of view. Thermal undulations have important effects on the system in the molecular scale [4] while can be neglected in the macroscopic level. The modified model is based on the description of Deserno *et al.* [30] *Thermal undulations exist and affect the stresses, because fluctuation induced corrugations shrink the projected surface area and thus contract the membrane.* This contraction can be modeled in another point of view. If we consider constant length criteria similar to the monolayer analysis, this shrinkage effect can be take into consideration by stress hardening of the membrane affect the variables of the system approximately same as the thermal undulation in the molecular point of view. Therefore, using the stress hardening model $\lambda = \lambda_0 (\sigma_x / \sigma_{x0})^n$ the modified model of the bilayer membrane is obtained. It should be noted that the bilayer membrane profiles of Figs.(4.15) and (4.16) are also obtained using the modified model.

The explained modified model is used to verify the presented solution by employing the results of Deserno *et al.* [30]. The verified results presented in Figs. (4.17) and (4.18) include variations of energy of the system and buckling load with respect to the dimensionless parameter $\gamma = (L_0 - L_x) / L_0$. It is illustrated in these figures that the results of continuum model of this project is approximately coincide with the energy-based results of [30]. Therefore, it can be concluded that the obtained model can be used as a promising model of the bilayer buckling phenomenon.

In addition to the verification of the results shown in Figs.(4.17) and (4.18), the incompressibility of the bilayer membrane is also investigated and the diagrams for the different applied buckling loads are presented in Fig.(4.19). Another variable is defined as incompressibility error $(d_0 - d) / d_0$ where d_0 and d are he distances of the two similar nodes in the layers of the membrane, respectively. As it is shown in Fig.(4.19), the incompressibility error is so small which can be considered as strength of the presented model of the bilayer membrane.

4.3 Dynamic analysis of membrane

In addition to the static analysis of membrane, time dependency of the considered phenomenon has special worth. In any system in different scales, micro or macro, dynamic modeling is so important and also complex with respect to static analysis. By employing dynamic analysis, variations of different variables of the system can be investigated with respect to time. These variations which can be linear or nonlinear are helpful not only to understand the natural or artificial systems but also to design or fabricate new ones properly.

As the first step, the presented mathematical modeling and numerical analysis is verified using the result of [74] about time variation of maximum deflection of a cantilever beam under a transverse step load (Fig.(4.20)). It is obvious that the presented model is well defined and its result for the cantilever beam problem has just a little difference with the result of [74]. In this case the concentrated load is applied vertically to the end of the beam and its dimensionless value is considered to be $F_y = 0.5$ to be compatible with the considered system of [74]. In addition, the dimensionless material parameters are chosen as $\lambda = 1$, $\rho = 1$, $J = 0.1$, $C = 6.3$ and $D = 0.1$. Henceforth, all of the diagrams are obtained base on these parameter values unless another values are mentioned in each case. As it is mentioned, time variation of different variables of any system should be considered as their important characteristics. In the buckling phenomenon of the considered monolayer membrane, maximum deflections for the system are primarily important and their time dependency are illustrated in Figs.(4.21) and (4.22) for two lengths and different buckling loads applied on the membrane. It is obviously shown that there is an important difference between these diagrams and the diagram of the cantilever problem based on transverse load. The variation of maximum deflection of the membrane in the beam problem is approximately linear in the beginning part of the diagram (Fig.(4.20)) while the diagrams of Figs.(4.21) and (4.22) related to the buckling problem has a delay in th starting point of deflection. In the case of transverse load, the applied load and direction of deflection are the same resulting in the shown behavior of the system. On the other

hand, in the buckling problem they are not in the same direction and the membrane should slowly deflect to reach a threshold which cause the bending moment of the applied load affect the deflection of the membrane and the rapid variation region starts. Because of the described buckling behavior, there are approximately two curvature in the y_{\max} – time diagrams including the positive one in the beginning part of the rapid growth region and the negative one at the end of the region. Moreover, the effects of the length and the applied buckling loads are illustrated in these diagrams. It is shown that by increasing the applied load, y_{\max} increases similar to the steady state model while the time required for the system to reach its steady state value decreases. It is also shown that the growth of the maximum deflection is faster for the smaller membrane and the starting point of the rapid growth regions of the diagrams of Fig.(4.22) correspond to shorter times.

In order to clarify the effects of the applied buckling load and dimensionless stiffness on the time variation of the buckling of the membrane, T_{steady} as the time required for the system to reach its steady state versus P_x and λ are presented in Figs.(4.23) and (4.24), respectively. As it is described before, T_{steady} decreases by increasing the applied buckling load. The load dependency of steady state time is not linear and the variations decreases by increasing the applied load (Fig.(4.23)). Moreover, the effects of λ on the steady state time is shown in Fig.(4.24). This dependency is also nonlinear. The dimensionless T_{steady} grows by increasing the stiffness and there is no limit for this parameter. It seems that by increasing the stiffness, it grows so that reaches a limit where the steady state time can be considered as infinity, e.g. there is no buckling.

Bode diagrams are among the useful ones in order to investigate dynamic behavior of a system. We used this helpful diagram to show the behavior of the system in frequency domain (Fig.(4.25)). It is shown that there is a jump in the frequency 10^0rad/s and the system is stable before this point. In addition, in the frequency greater than 10^0rad/s the system has a jump to reach to another region and grows smoothly in that region. This specific behavior is also based on the behavior of the system in buckling phenomenon. It should be noted that the magnitude and phase difference are shown in dB and deg units which are usual in presenting Bode diagrams.

As a more complicated and interesting problem, dynamic buckling of the heterogeneous membrane is also solved and the results are presented here. The heterogeneity can exist in a membrane like the proteins or other molecules exist in lipid bilayers. Hence, by investigating this problem, we can go one step further in investigating a more realistic problem. The heterogeneity of the system can be defined based on different material properties of the system. In all of the results presented in this part, a small region $l_h = 0.2$ with a different value of one of the properties of the system such as dimensionless stiffness λ is put in the domain. Some of the results are based on the effects of changing the position of this part and the other ones related to the different behavior of the system by considering this small region in the critical location in the domain.

The effects of existence of the small heterogeneous region with different λ , as an important material property of the system, on the steady state time of the buckling phenomenon are illustrated in Figs.(4.26) and (4.27). It is clearly shown that there is a extremum in the diagrams located at the middle of the diagram. It means that the most important position of the heterogeneous region with different λ is the middle of the membrane. As it is shown in Fig.(4.26), existence of the heterogeneous part with $\lambda = 10/9$ which is less than the stiffness of the whole membrane causes increasing T_{steady} and the maximum is happened when it is located at the middle of the membrane. It is also shown that it is more effective for larger applied buckling loads. The existence of a softer heterogeneous part is also shown in Fig.(4.27). The effect is opposite to the harder part and causes decreasing the time. Similar to the diagrams of Fig.(4.26), there is a extremum in every diagram which located in the middle of the interval. Therefore, similar to the heterogeneous static results, it can be concluded that middle of the membrane is the most critical region for existence of the heterogeneous part in the system. In the static model, its effects on maximum deflection and in this case its effects on steady state time are investigated. In order to obtain the effects of the stiffness of this heterogeneous region on the membrane, the diagram of T_{steady} versus λ_h is obtained (Fig.(4.28)). In this diagram, the heterogeneous part is located in the critical region, e.g. middle of the membrane, and its stiffness values are changed between 0.8 and 1.2. As it is shown in this figure, increasing the stiffness of the heterogeneous part

corresponds to increasing the steady state time of the buckling of the membrane. It can be also concluded that the dependency of the T_{steady} on λ_h can be approximately considered as linear.

The other properties of the membrane are just appeared in the dynamic analysis and related to the dynamic behavior of the membrane. As the next step, the effects of existence of a heterogeneous part with different ρ as one of these dynamic parameters are investigated. The diagrams of T_{steady} versus position of the beginning of the heterogeneous part a are shown in Fig.(4.29). In these diagrams, density of the heterogeneous part is considered to be $\rho_h = 2\rho$. In addition, similar diagrams for a heterogeneous part with $\rho_h = 0.5\rho$ are illustrated in Fig.(4.30). In both figures, the extremum of the diagram is located in a different position than the one obtained for heterogeneous part with different λ . The extremum is in $a = 0.34$. The profiles of Figs.(4.5) and (4.6) clarify the reason. There is a region in the buckling profiles can be considered approximately linear centered by the middle of the membrane. If we consider an average, $a = 0.28$ is the start of this small region and can be considered as the critical point for dynamic parameter ρ . In order to clarify the effects of ρ_h on the dynamic behavior of the membrane, T_{steady} versus ρ_h is presented in Fig.(4.31). It is shown that even it affects the behavior of the system (linearly) its effect is so small. The variation of T_{steady} in this diagram clarify small effect of this parameter on the dynamic behavior of the system.

In addition to ρ_h , the effects of bending damping C_h is also taken into consideration. Figures (4.32) and (4.33) show variation of steady state time of the buckling of the membrane with respect to the start point of the heterogeneous part. In Fig.(4.32), C_h is considered to be half of the bending damping of the membrane and it is considered to be two time C for the diagrams presented in Fig.(4.33). It is clearly shown in these diagrams that the critical point is located at the middle of the membrane in this case. Increasing the applied load causes increasing T_{steady} as illustrated before. On the basis of the presented figures it can be easily concluded that the system reaches to the steady state condition at the highest time stages if they consist of heterogeneous part with larger bending damping. This behavior is also shown in Fig.(4.34) determining the dependency of T_{steady} on bending damping of the

system. This behavior is based on the definition of damping which dissipate the energy of the system. It causes the system to change from the initial configuration smoothly to the final configuration. It is also can be seen that bending damping has a big effect on the variation of the steady state time and can easily change the dynamic behavior of the membrane.

As the last parameter, different values of D_h are chosen to investigate the effects of this parameter as the heterogeneity of the system. In Figs.(4.35) and(4.36), variations of steady state time with respect to the start point of the heterogeneous region are illustrated for the membrane under different buckling loads. Similar to the heterogeneous membrane include the heterogeneity of density, the extremums of the diagrams are located at the same point $a = 0.28$. This point represent the maximum values and minimum values of T_{steady} in diagrams of Fig.(4.35) in which $D_h = 0.5D$ and Fig.(4.36) in which $D_h = 2D$, respectively. The effect of the different values of D_h on the dynamic behavior of the system is shown in Fig.(4.37) which clarify the importance of this parameter. It is shown that by small changes of this parameter, steady state time vary in a large range.

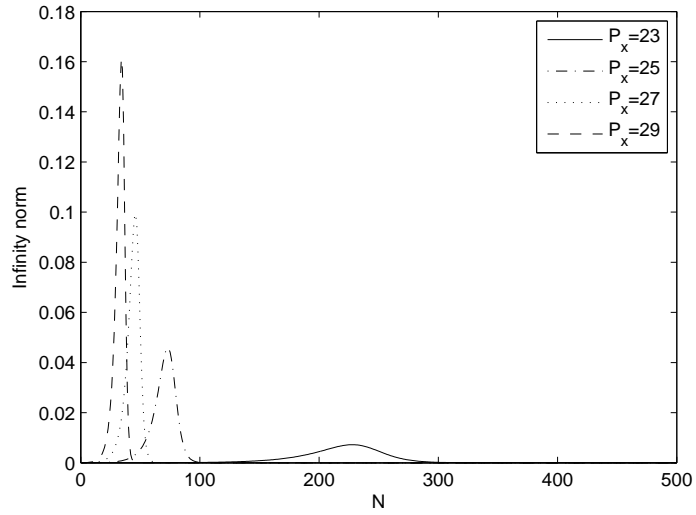


Figure 4.1: N_∞ versus number of iterations for different applied loads on a membrane with half length $L = 2/3$.

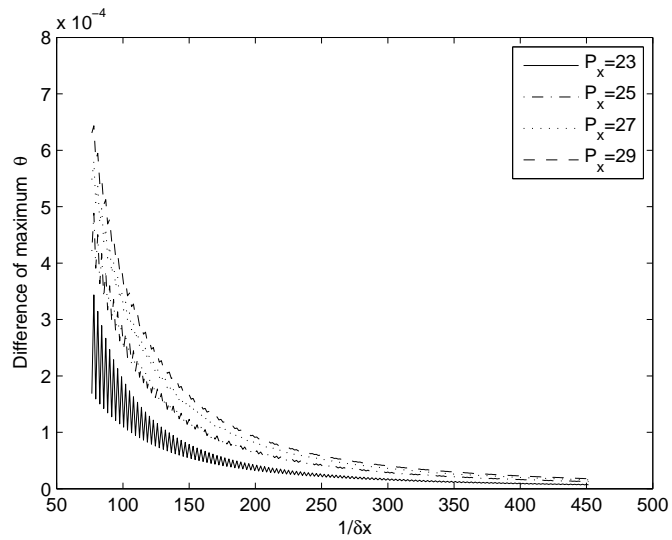


Figure 4.2: Variation of difference of maximum slope based on two considered δx in a sequence with respect to $1/\delta x$.

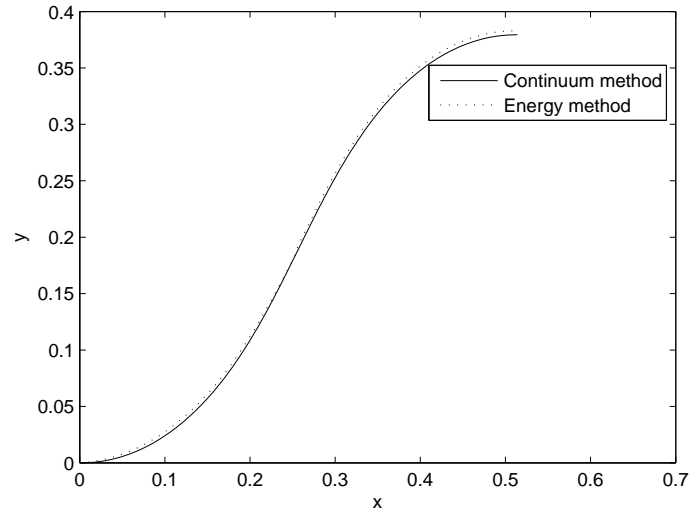


Figure 4.3: Comparison of the presented solution and energy-based solution [46] for $L = 2/3$.

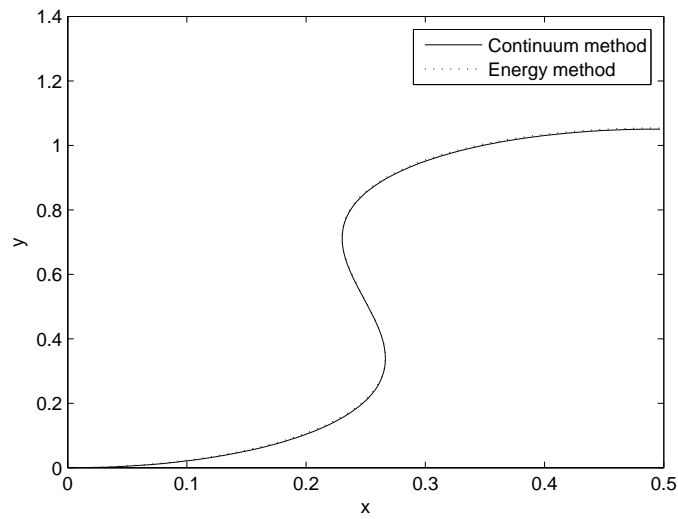


Figure 4.4: Comparison of the presented solution and energy-based solution [46] for $L = 4/3$.

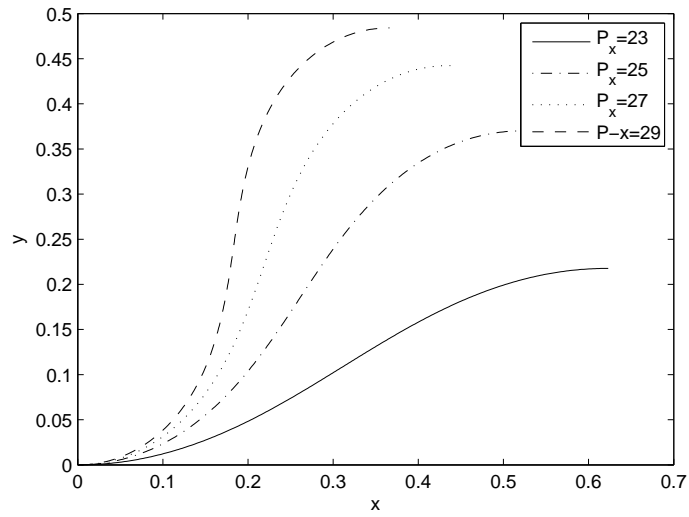


Figure 4.5: Membrane profiles after buckling for different applied loads and $L = 2/3$.

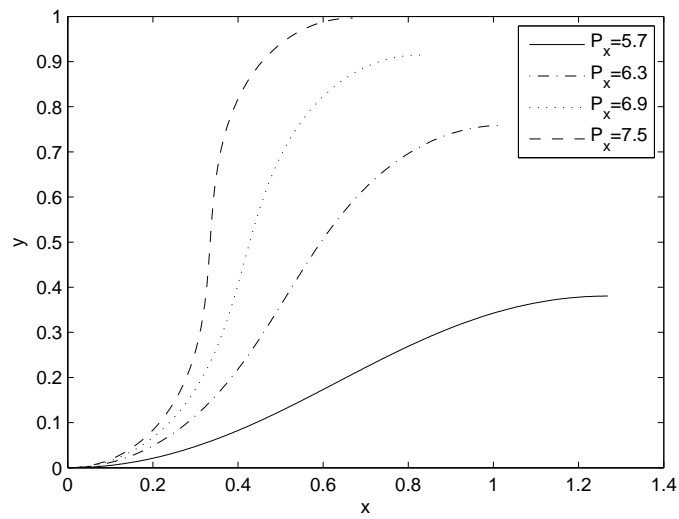


Figure 4.6: Membrane profiles after buckling for different applied loads and $L = 4/3$.

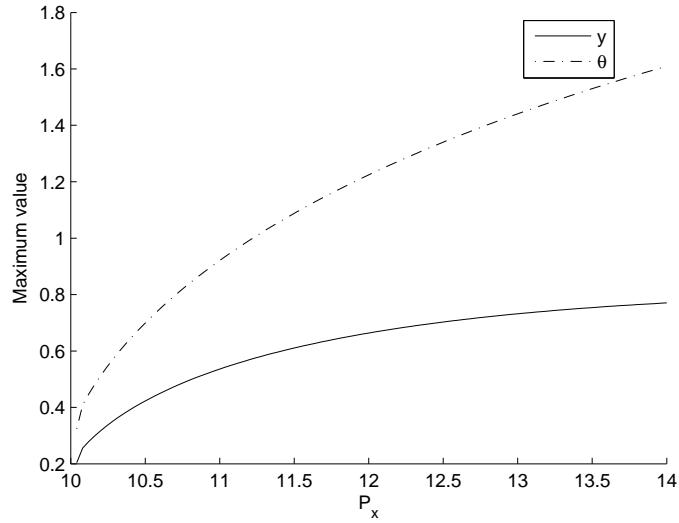


Figure 4.7: Variation of y_{max} and θ_{max} with respect to applied load for a membrane with half length $L = 1$.

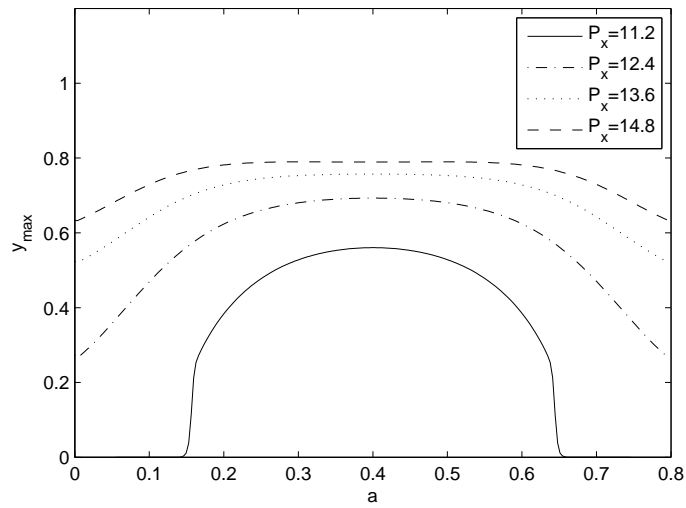


Figure 4.8: Variation of y_{max} with respect to the position of the small softer part ($l_h = 1/5$) of the heterogenous membrane ($L = 1$) under different horizontal loads.

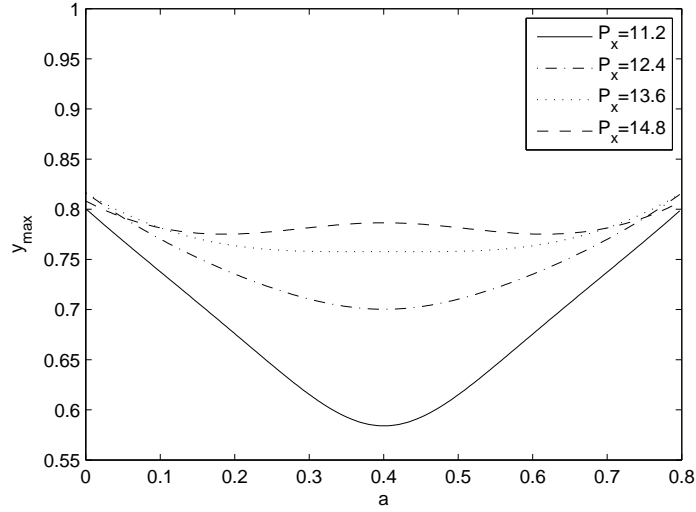


Figure 4.9: Variation of y_{max} with respect to the position of the small stiffened part ($l_h = 1/5$) of the heterogenous membrane ($L = 1$) under different horizontal loads.

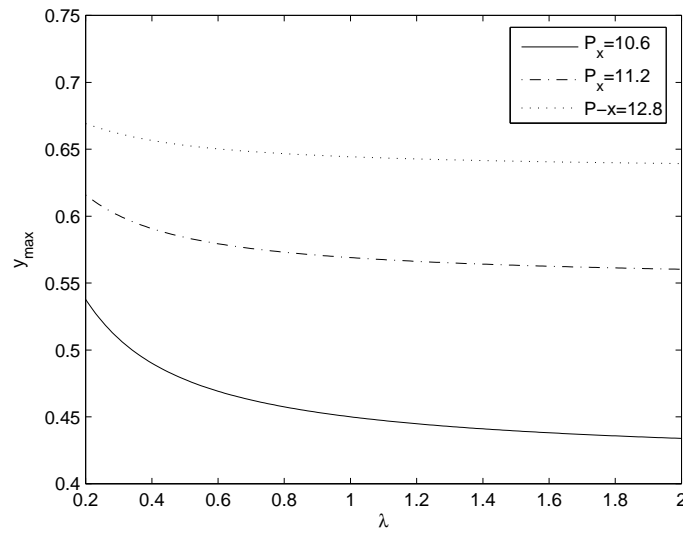


Figure 4.10: y_{max} versus λ for a heterogenous membrane, heterogeneity located at the middle, with half length $L = 1$ under different horizontal loads.

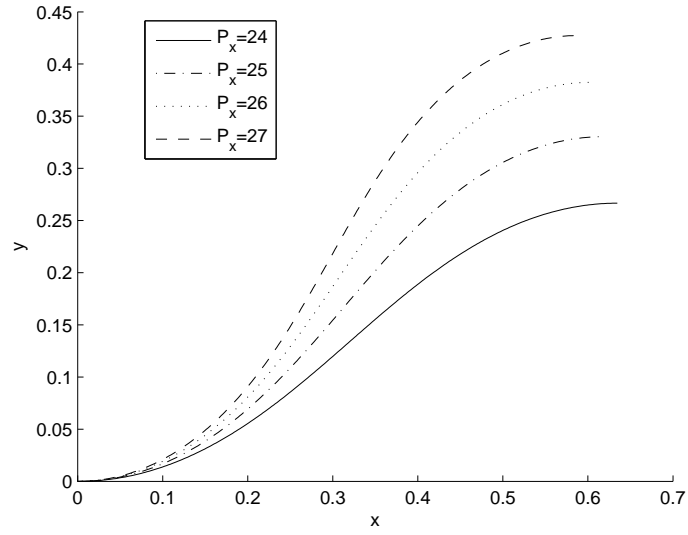


Figure 4.11: profiles of circular membrane after buckling for different applied loads and $L = 2/3$.

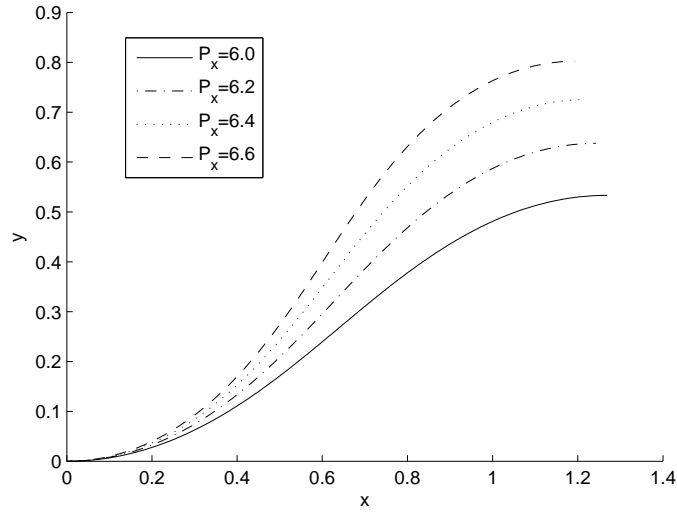


Figure 4.12: profiles of circular membrane after buckling for different applied loads and $L = 4/3$.

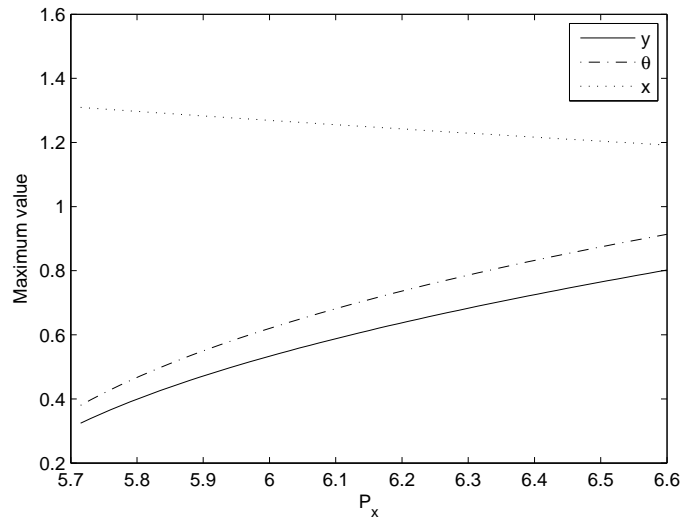


Figure 4.13: Variations of θ_{max} , x_{max} and y_{max} with respect to P_x .

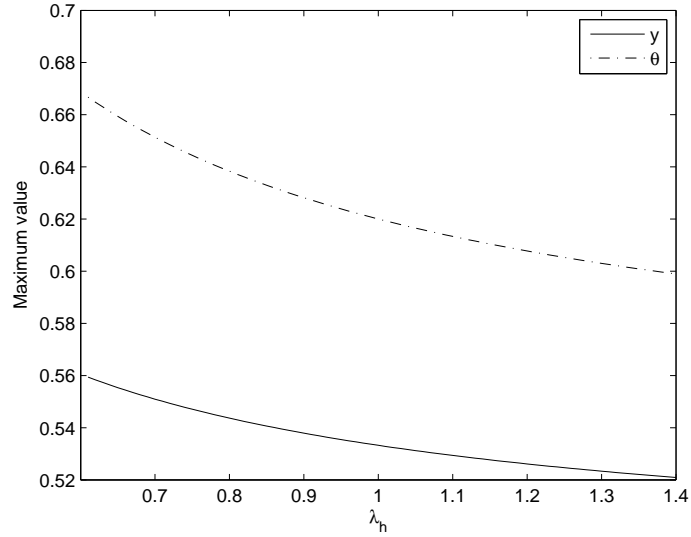


Figure 4.14: Variations of y_{max} and θ_{max} with respect to non-dimensional stiffness of the middle part of the membrane with length $l_h = 1/5$.

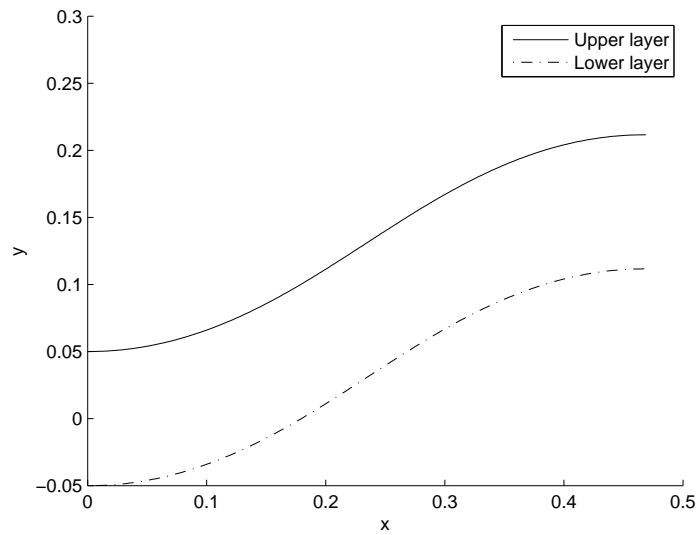


Figure 4.15: Profiles of the layers of the bilayer membrane with half length $L = 1/2$ and under applied load $P_x = 41$.

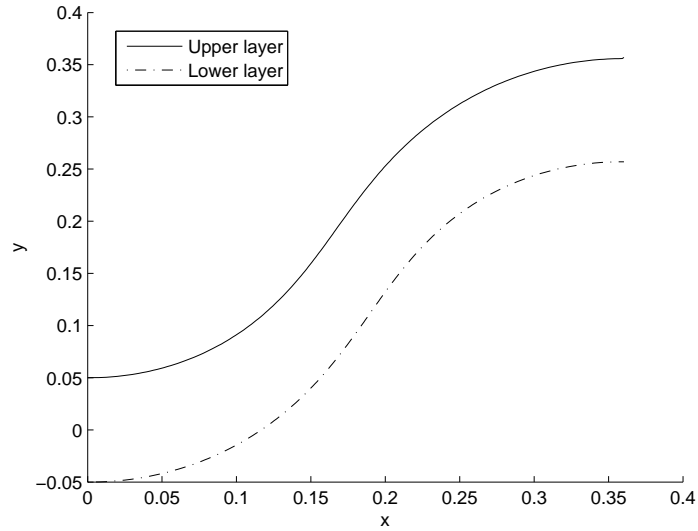


Figure 4.16: Profiles of the layers of the bilayer membrane with half length $L = 1/2$ and under applied load $P_x = 47$.

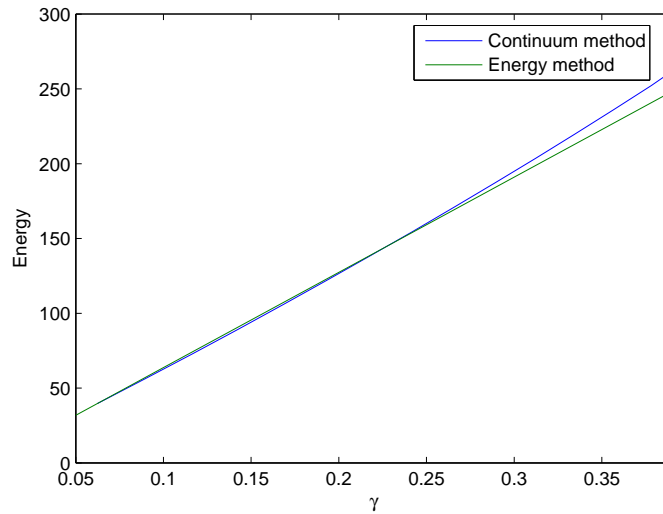


Figure 4.17: Energy of the bilayer membrane versus γ using both continuum method of this project and energy method of [30].

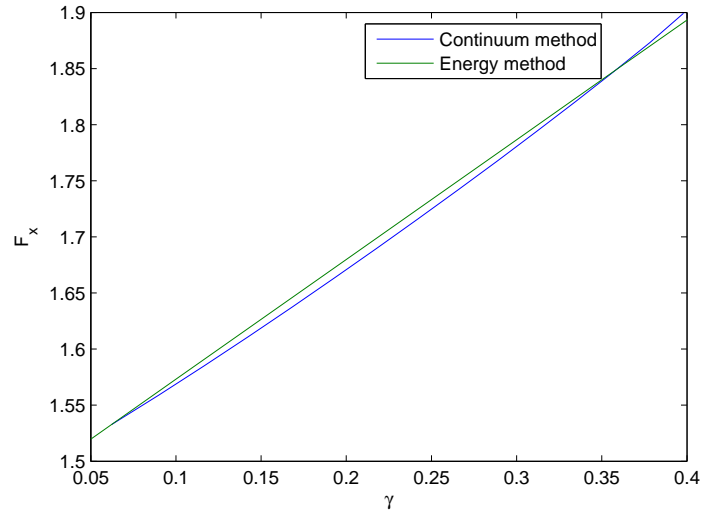


Figure 4.18: Variation of F_x applied to the bilayer membrane with half length $L = 1/2$ with respect to γ using both continuum method of this project and energy method of [30].

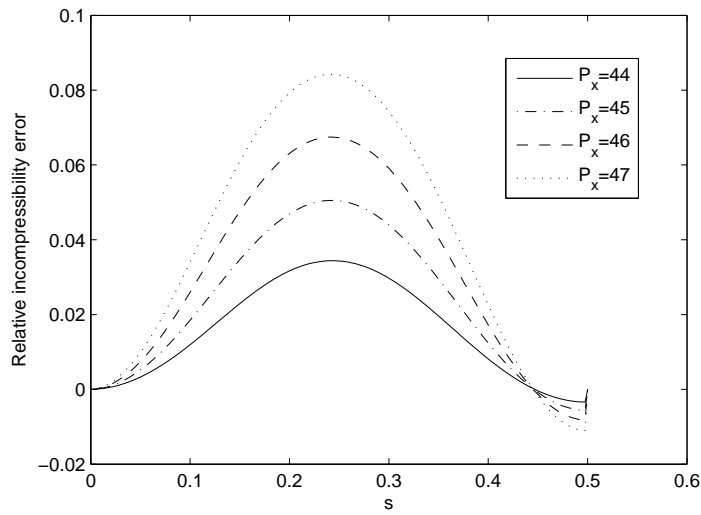


Figure 4.19: Relative incompressibility error in the bilayer membrane with half length $L = 1/2$ under different applied buckling loads.

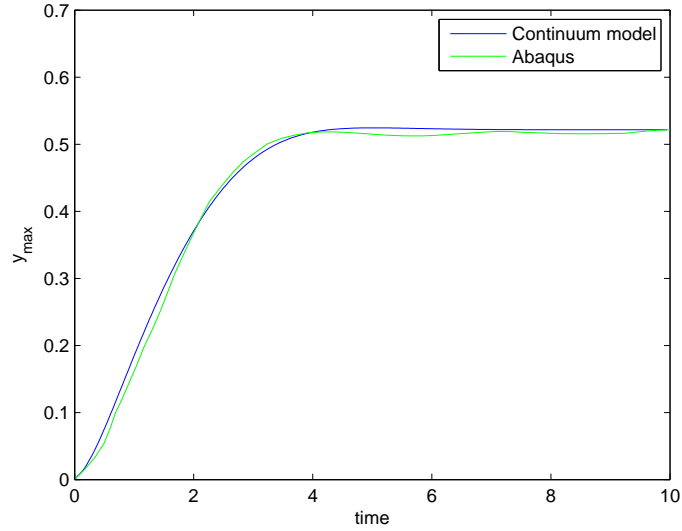


Figure 4.20: Variation of y_{max} with respect to time for a cantilever beam subjected to a step loading as verification of the dynamic model [74].

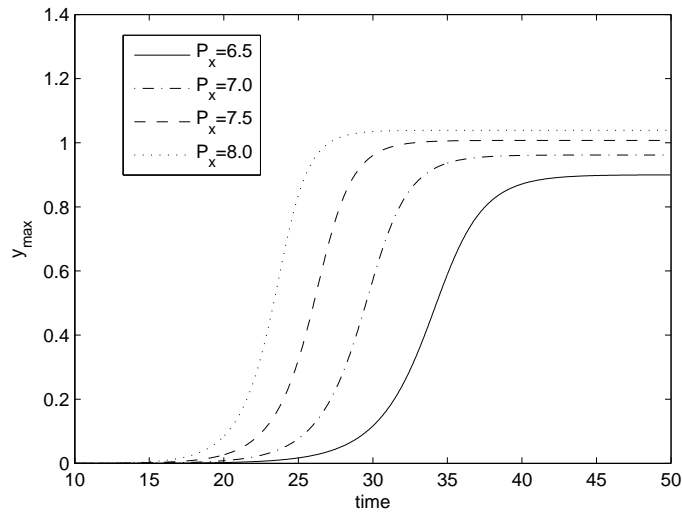


Figure 4.21: Variation of maximum deflection with respect to time for the monolayer membrane with half length $L = 4/3$ under different applied buckling loads.

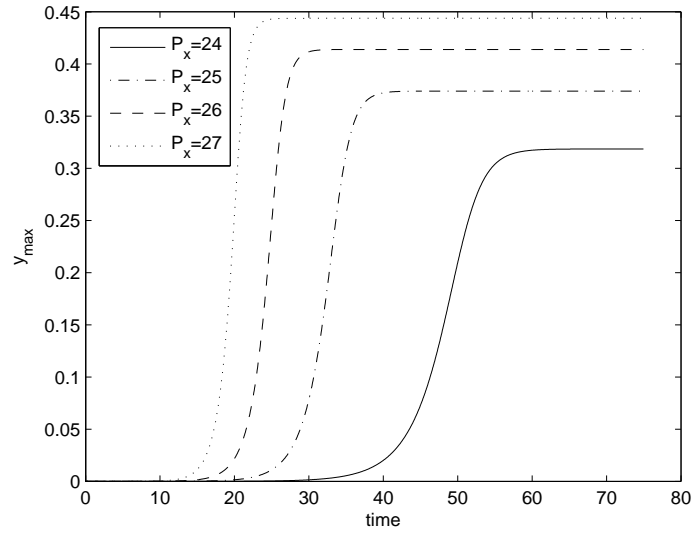


Figure 4.22: Variation of maximum deflection with respect to time for the monolayer membrane with half length $L = 2/3$ under different applied buckling loads.

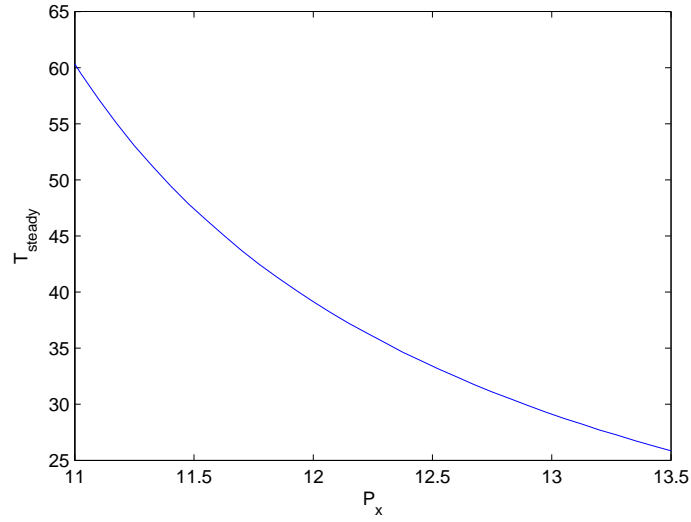


Figure 4.23: T_{steady} versus applied horizontal load P_x for the membrane with half length $L = 1$.

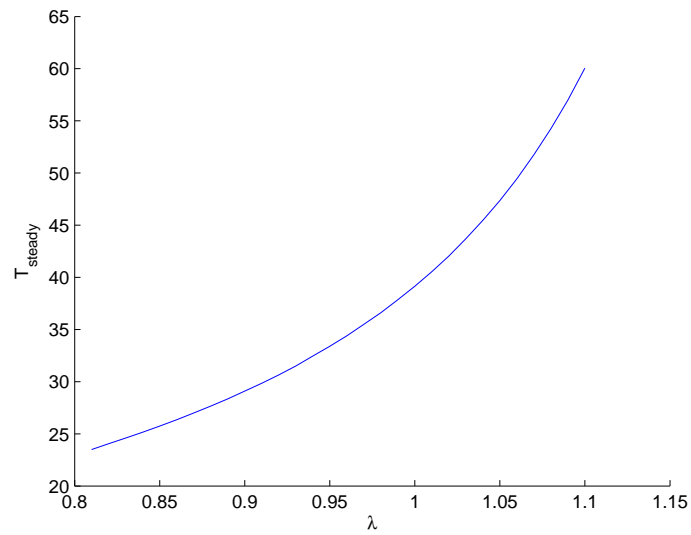


Figure 4.24: T_{steady} versus dimensionless stiffness λ for the membrane with half length $L = 1$.

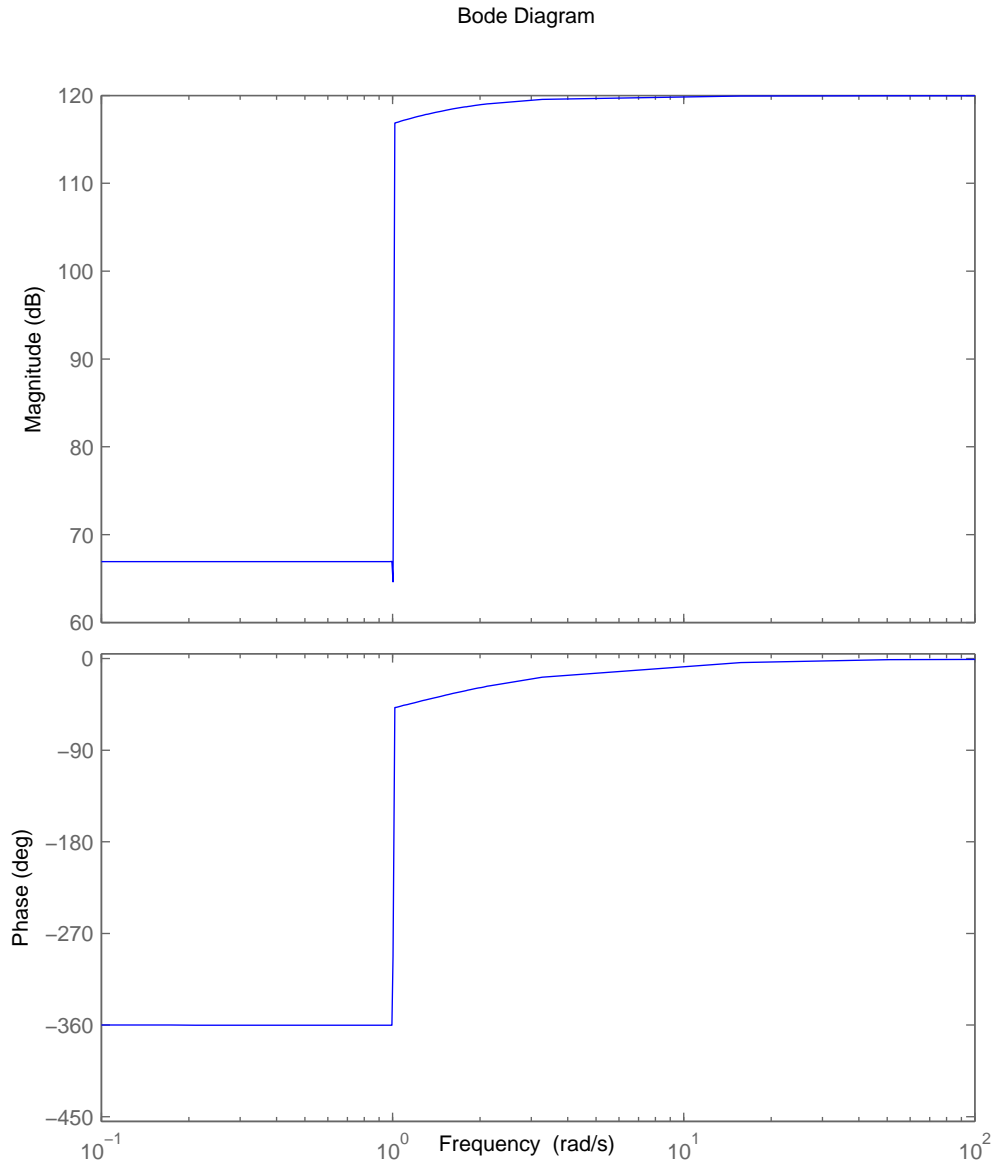


Figure 4.25: Bode diagram of the monolayer membrane with half length $L = 1$. Magnitude (dB) and phase (deg) of y_{max} with respect to frequency of the system (rad/s)

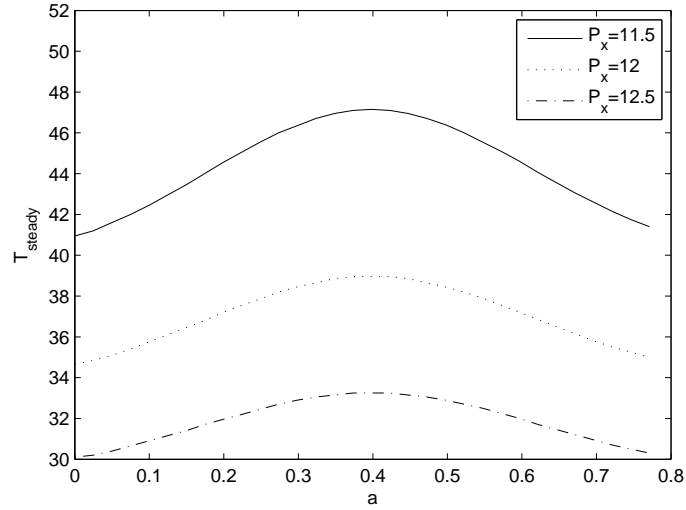


Figure 4.26: Variation of T_{steady} of the membrane with half length $L = 1$ with respect to the beginning position of the heterogeneous part with $\lambda_h = 10/9$ and $l_h = 0.2$.

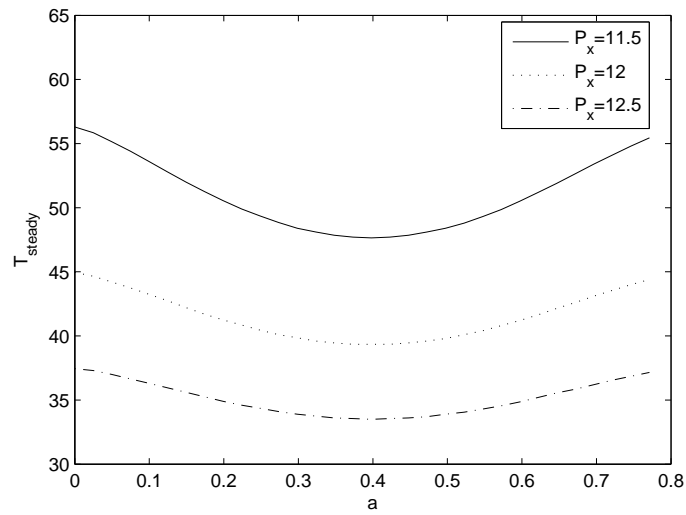


Figure 4.27: Variation of T_{steady} with respect to the beginning position of the heterogeneous part with $\lambda_h = 9/10$ and $l_h = 0.2$.

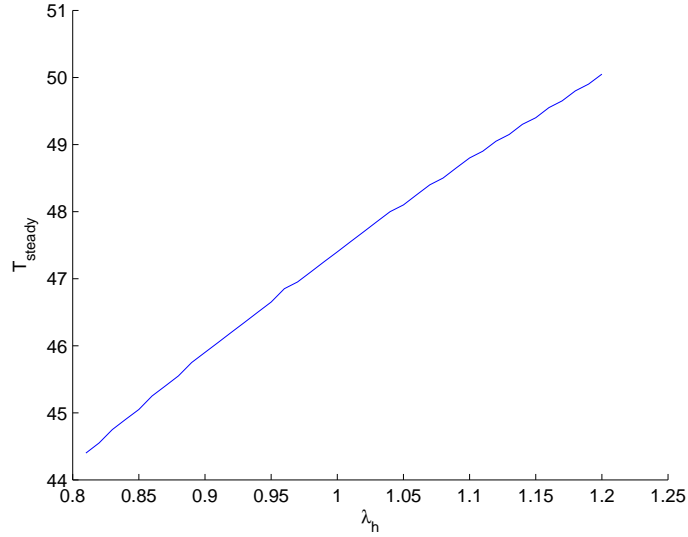


Figure 4.28: T_{steady} versus heterogeneous stiffness λ_h for the heterogeneous part located in the middle of the considered half membrane.

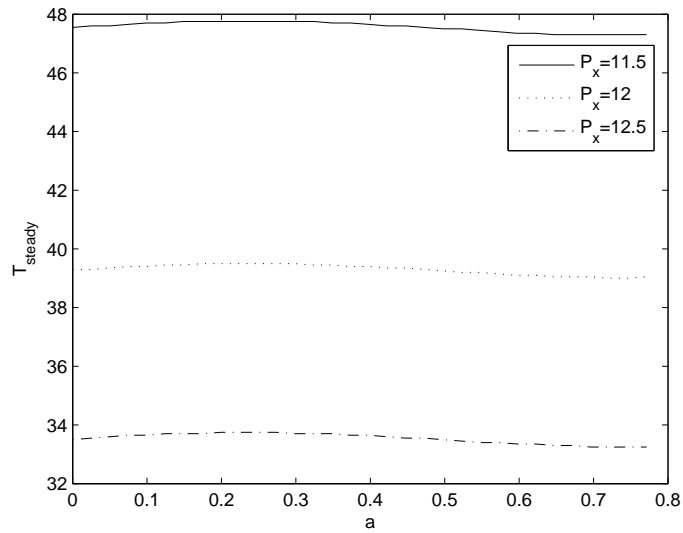


Figure 4.29: Variation of T_{steady} of the membrane with half length $L = 1$ with respect to the beginning position of the heterogeneous part with $\rho_h = 2\rho$ and $l_h = 0.2$.

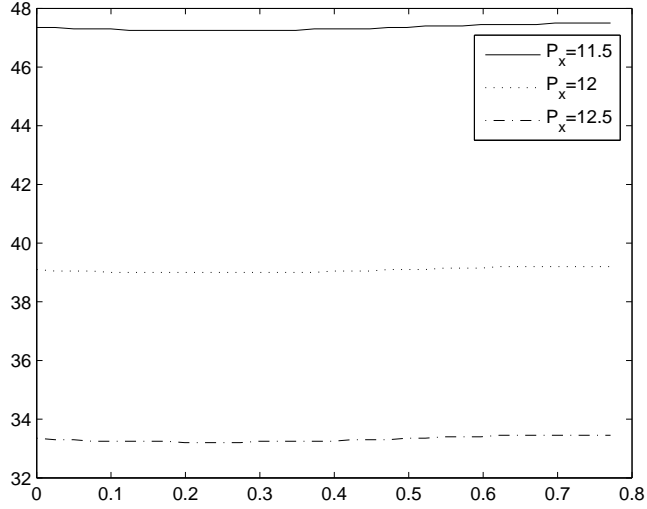


Figure 4.30: Variation of T_{steady} of the membrane with half length $L = 1$ with respect to the beginning position of the heterogeneous part with $\rho_h = 0.5\rho$ and $l_h = 0.2$.

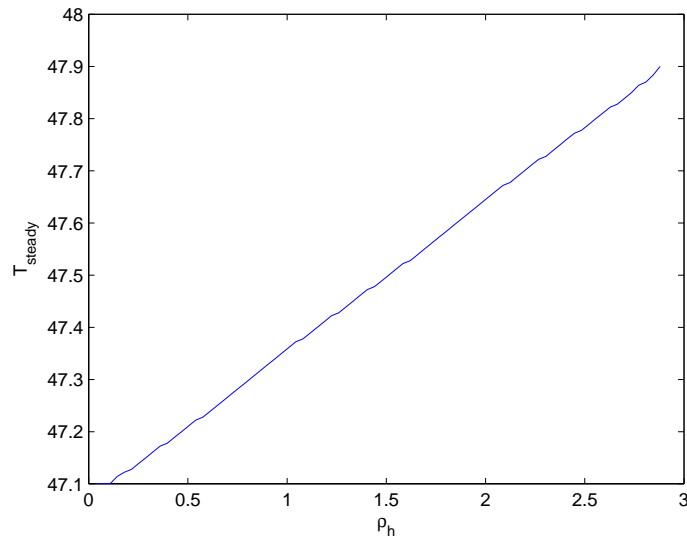


Figure 4.31: T_{steady} versus heterogeneous density ρ_h for the heterogeneous part located in $a = 0.34$ of the considered half membrane.

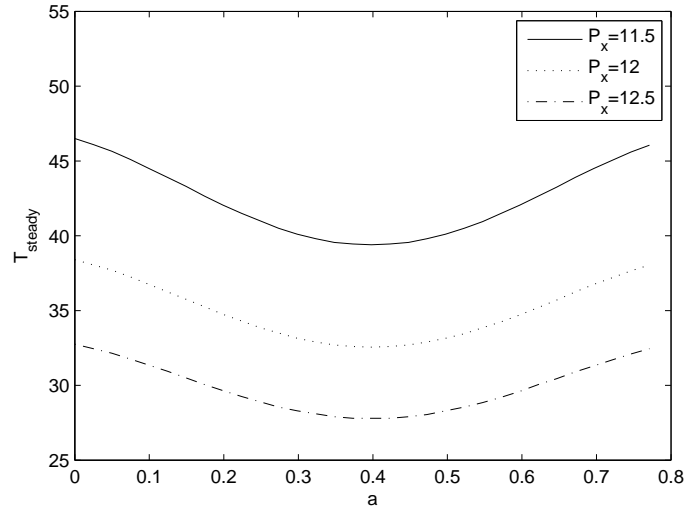


Figure 4.32: Variation of T_{steady} of the membrane with half length $L = 1$ with respect to the beginning position of the heterogeneous part with $C_h = 0.5C$ and $l_h = 0.2$.

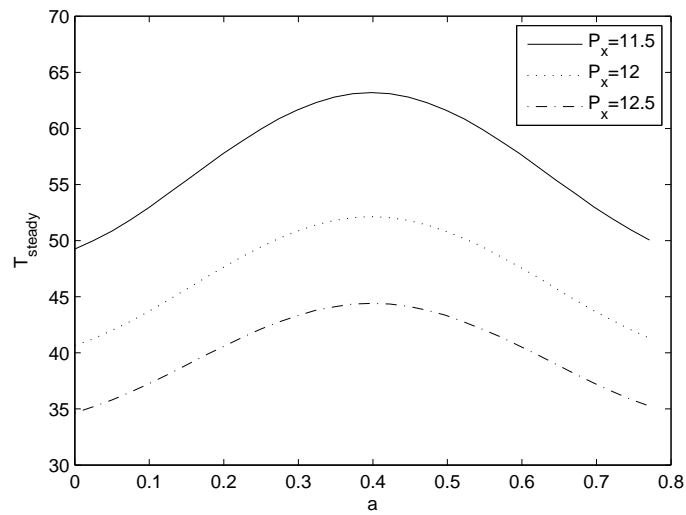


Figure 4.33: Variation of T_{steady} of the membrane with half length $L = 1$ with respect to the beginning position of the heterogeneous part with $C_h = 2C$ and $l_h = 0.2$.

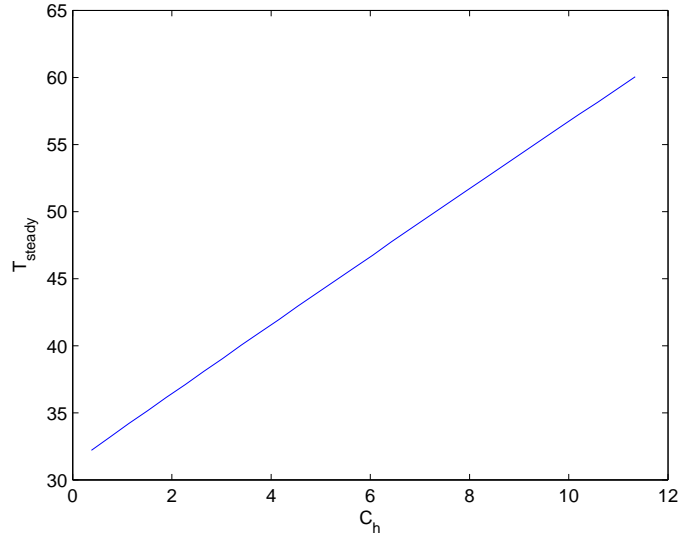


Figure 4.34: T_{steady} versus heterogeneous density C_h for the heterogeneous part located in $a = 0.4$ of the considered half membrane.

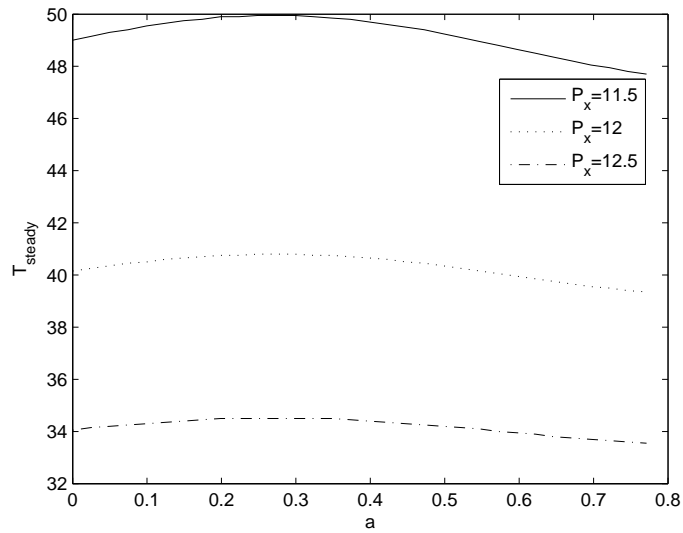


Figure 4.35: Variation of T_{steady} of the membrane with half length $L = 1$ with respect to the beginning position of the heterogeneous part with $D_h = 0.5D$ and $l_h = 0.2$.

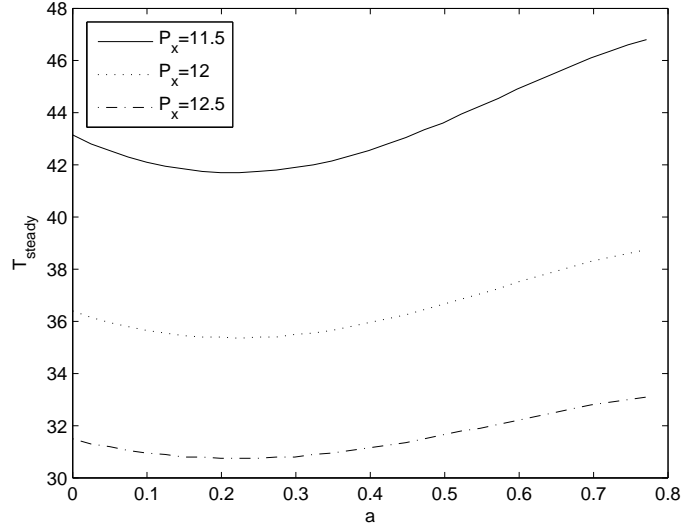


Figure 4.36: Variation of T_{steady} of the membrane with half length $L = 1$ with respect to the beginning position of the heterogeneous part with $D_h = 2D$ and $l_h = 0.2$.

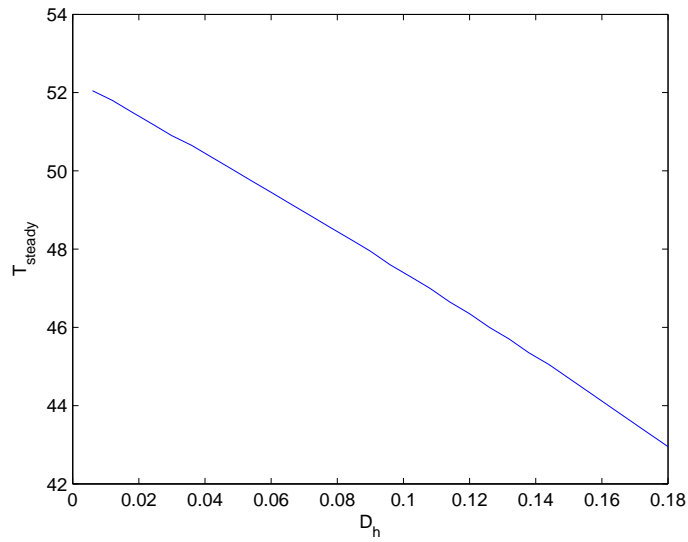


Figure 4.37: T_{steady} versus heterogeneous density D_h for the heterogeneous part located in $a = 0.34$ of the considered half membrane.

Chapter 5

Conclusion

Different analytical models are presented in this project to model the biomembranes as elastic domains. The Euler-Bernoulli constitutive law is used to obtain different models including one-dimensional and circular monolayer membrane as well as bilayer membranes in the steady state conditions. The dynamic behavior of the monolayer membrane is modeled as well. The dimensionless equations of the investigated problems including nonlinear ordinary and integro partial differential equations are obtained let us to present more general results can be used to study different biomembranes with different properties and dimensions. The equations are discretized using different finite difference schemes. The matrix forms of the discretized equations are then solved to obtain the solution of each problem.

Different solutions obtained employing the presented models and using the described numerical methods are used to show the behavior of the membranes in buckling phenomenon. As one of the most important physical phenomenon studied so much during the last decades, the presented models and solution procedures can be considered as new approaches to investigated it for homogeneous and heterogeneous domains.

As the primary step, convergence and grid-independency of the numerical procedure is presented to be sure about the employed procedure. It should be mentioned that the re-

sults of each problems is verified using the available results in the literature. Buckling of one-dimensional and axisymmetric membranes are studied as the two well-known problems in the steady state condition. The profiles of the membrane under different concentrated buckling load are shown. Moreover, the dependency of the maximum deformation and slope of the membrane as two important parameters are illustrated. The effects of existence of a small heterogeneous region in the system is studied and the critical location is obtained in each case. The effects of the properties of this small region is investigated as well.

The static analysis of bilayer membrane is also presented as more complicated problem because of the incompressibility criteria between the layers. The profiles of the membrane and the effects of stiffness of the layers are investigated. In addition, the incompressibility of the system is studied and it is clearly shown that the obtained solution can be considered as an accurate and promising tool to investigate the buckling phenomenon in bilayer membranes.

As the last problem of the project, dynamic behavior of the homogeneous and heterogeneous biomembrane is investigated. The variations of different variables of the model with respect to time are shown. The membrane starts to deflect rapidly in specific time stage. This stage can be changed based the applied load and properties of the membrane. The effects of the dimensionless parameters such as bending dissipation of the system on the behavior of the membrane is well studied. Moreover, effects of existence of different heterogeneous regions with different properties are clarified as well as the dependency of the behavior of the system on the position of the small heterogeneous regions.

It can be concluded that the presented models, numerical procedure can be considered as promising tools to investigate the static and dynamic behavior of homogeneous and heterogeneous monolayer and bilayer membranes.

Chapter 6

Outlook

The importance and abilities of the presented models are well clarified throughout the project. Because of the flexibility of the presented approaches, they can be extended to become more realistic step by step. The effects of membrane thickness and heterogeneity in the transverse direction can be studied. In addition, the presented methods can be developed to study two and three dimensional systems with more complicated geometries. The slip of the layers of the bilayer membranes can be added to the models as well. These extensions can be helpful to obtain more general models can be used to investigate the real biological membranes without any simplification analytically.

Appendix A

Modeling of biomembrane using energy method

The mathematical modeling of the membrane based on the energy method [30] is presented here. The procedure described here are based on the mathematical modeling of [30] and just some missing parts are added to clarify the procedure. This model is based on the analysis of the membrane behavior using the energy of the system. In the case of bending of a membrane, the energy function include two terms based on bending and Gaussian curvatures [4]. Hence, the energy functional can be written as follows

$$\varepsilon [S] = \int_S dA \left[\frac{1}{2} \kappa (K - K_0)^2 + \bar{\kappa} K_G \right] \quad (\text{A-1})$$

where

$$K = c_1 + c_2, \quad K_G = c_1 c_2 \quad (\text{A-2})$$

One the basis of the considered assumption about one-dimensional membrane, the following relations can be written for the principle curvatures of the membrane after deflection

$$c_1 = \frac{d\theta}{ds}, \quad c_2 = 0 \quad (\text{A-3})$$

In order to present similar equations to [30], ψ is used as the slope of the membrane at each section instead of θ . On of the curvatures is equal to zero $c_2 = 0$, there is no Gaussian term in the energy functional in the considered system. Now, we can write the energy functional using ψ as the variable of the system and its derivatives as follows

$$\varepsilon [S] = \int_S dA \left[\frac{1}{2} \kappa \dot{\psi}^2 + f_x \left[\cos \psi - \frac{L_x}{L} \right] \right] \quad (\text{A-4})$$

where f_x is the Lagrange multiplier and should be used to ensure that the horizontal length of the membrane is fixed to be equal to L_x . It should be noted that this parameter play the same role as p_x in the continuum model of this project. The boundary conditions of the membrane is considered to be $\psi(0) = \psi(L)$.

The obtained energy functional Eq. (A-1) can be put in the functional variation procedure as follows

$$\begin{aligned} F &= \frac{1}{2} \kappa \dot{\psi}^2 + f_x \left[\cos \psi - \frac{L_x}{L} \right], \quad \frac{\partial F}{\partial \psi} - \frac{d}{ds} \frac{\partial F}{\partial \dot{\psi}} = 0 \\ \Rightarrow -f_x \sin \psi - \frac{d}{ds} (k \dot{\psi}) &= 0 \Rightarrow k \ddot{\psi} + f_x \sin \psi = 0 \end{aligned} \quad (\text{A-5})$$

Therefore, $\psi(s)$ satisfies the Euler-Lagrange differential equation

$$\ddot{\psi} + \lambda^{-2} \sin \psi = 0, \quad \lambda^2 = \frac{\kappa}{f_x} \quad (\text{A-6})$$

If we multiply $\dot{\psi}$ on both sides of the Eq. (A-6), the following equations can be easily obtained

$$\dot{\psi} \ddot{\psi} + \lambda^{-2} \dot{\psi} \sin \psi = 0 \Rightarrow \frac{d}{ds} \left(\frac{1}{2} \dot{\psi}^2 - \lambda^{-2} \cos \psi \right) = 0 \quad (\text{A-7})$$

resulting in the following relation

$$\frac{1}{2} \dot{\psi}^2 - \lambda^{-2} \cos \psi = \text{const.} \quad (\text{A-8})$$

It is obvious that within the average plane we can consider $\dot{\psi} = 0$ to simplify Eq. (A-8) as follows

$$\begin{aligned} \frac{1}{2} \dot{\psi}^2 - \lambda^{-2} \cos \psi &= -\lambda^{-2} \cos \psi_i \\ \Rightarrow \dot{\psi} &= \lambda^{-1} \sqrt{2 (\cos \psi - \cos \psi_i)} \end{aligned} \quad (\text{A-9})$$

Now, we can substitute the obtained relation for $\dot{\psi}$ (Eq.(A-9)) into Eq. (A-4) to simplified this equation as follows

$$\begin{aligned}
\varepsilon [S] &= \int_S dA \left[\frac{1}{2} \kappa \lambda^{-2} (2 \cos \psi - 2 \cos \psi_i) + f_x \left[\cos \psi - \frac{L_x}{L} \right] \right] \\
\Rightarrow \varepsilon [S] &= \int_S dA \left[f_x (\cos \psi - \cos \psi_i) + f_x \left[\cos \psi - \frac{L_x}{L} \right] \right] \\
\Rightarrow \varepsilon [S] &= L_y [f_x L_x - f_x L \cos \psi_i] \Rightarrow \varepsilon [S] = L_y f_x [L_x - L \cos \psi_i] \\
\Rightarrow \varepsilon [S] &= f_x A (2m - \gamma)
\end{aligned} \tag{A-10}$$

where $A = LL_y$ is the total area of the membrane and $\gamma = \frac{L-L_x}{L}$ is the dimensionless compressive strain. In addition, m is a trigonometric function can be obtained as follows

$$\begin{aligned}
L_x - L \cos \psi_i &= L \left(2m - 1 + \frac{L_x}{L} \right) \Rightarrow L_x - L \cos \psi_i = 2mL - L + L_x \\
\Rightarrow 2m &= 1 - \cos \psi_i \Rightarrow 2m = 1 - \left(1 - 2 \sin^2 \frac{\psi_i}{2} \right) \Rightarrow m = \sin^2 \frac{\psi_i}{2}
\end{aligned} \tag{A-11}$$

Moreover, the differential equation (Eq. (A-9)) can be written to the integral form in the well-known elliptic integral of the first kind as follows

$$\begin{aligned}
\sqrt{\cos \psi - \cos \psi_i} &= \sqrt{1 - 2 \sin^2 \frac{\psi}{2} - \cos \psi_i} \\
&= \sqrt{(1 - \cos \psi_i) - 2 \sin^2 \frac{\psi}{2}} \\
&= \sin \frac{\psi_i}{2} \sqrt{1 - \frac{1}{\sin^2 \frac{\psi_i}{2}} \sin^2 \frac{\psi}{2}}
\end{aligned} \tag{A-12}$$

and using $\dot{\psi} = \lambda^{-1} \sqrt{2 (\cos \psi - \cos \psi_i)}$

$$\Rightarrow \frac{1}{\sin \frac{\psi_i}{2}} \int \frac{d\psi}{\sqrt{1 - \frac{1}{\sin^2 \frac{\psi_i}{2}} \sin^2 \frac{\psi}{2}}} = \sqrt{2} \lambda^{-1} \int ds$$

Therefore, we can easily obtain the following equation using $\psi(s=0) = 0$

$$\frac{s}{\lambda} = F \left[\arcsin \left(m^{-1/2} \sin \frac{\psi}{2} \right), m \right] \tag{A-13}$$

resulting in the angle as a function of arc length

$$\psi(s) = 2 \arcsin \left[\sqrt{m} \operatorname{sn} \left[\frac{s}{\lambda}, m \right] \right] \quad (\text{A-14})$$

In addition, we can obtain the following relations for the $x(s)$ and $z(s)$

$$\begin{aligned} x(s) &= \int ds \cos \psi(s) \Rightarrow x(s) = 2\lambda E \left[\operatorname{am} \left[\frac{s}{\lambda}, m \right], m \right] - s \\ z(s) &= \int ds \sin \psi(s) \Rightarrow z(s) = 2\lambda\sqrt{m} \left(1 - \operatorname{cn} \left[\frac{s}{\lambda}, m \right] \right) \end{aligned} \quad (\text{A-15})$$

There are still two unknowns in the obtained equations including the characteristic length λ and the elliptic parameter m should be obtained to be able to solve the problem completely. There are two constraint in the system can be used to obtain eliminate these variables:

- $\psi(s)$ must have period L
- "When s has increased by L , x must have increased by L_x "

For the first constraint, we can write the following equations

$$\psi \left(\frac{L}{4} \right) = \psi_i, \text{ using Eq. (A-14)} \Rightarrow \frac{L}{4\lambda} = F \left[\frac{\pi}{2}, m \right] = K[m] \quad (\text{A-16})$$

The second constraint also results in the following equations

$$\frac{L_x}{4} = x \left(\frac{L}{4} \right), \text{ using Eq. (A-15)} \Rightarrow L_x = 8\lambda E[m] - L \quad (\text{A-17})$$

On the basis of the Eqs. (A-16) and (A-17), we have

$$\gamma_i = \frac{L - L_x}{L} = 2 \left(1 - \frac{E[m]}{K[m]} \right) \quad (\text{A-18})$$

If we expand the elliptic parameter m with respect to γ as $m(\gamma) = \sum_i a_i \gamma^i$ where the coefficients a_i can be obtained as follows using Eq. (A-18)

$$a_i = \frac{1}{i!} \lim_{m \rightarrow 0} \frac{\partial^{i-1}}{\partial m^{i-1}} \left[\frac{2}{m} \left(1 - \frac{E[m]}{K[m]} \right) \right]^{-i} \quad (\text{A-19})$$

Another method is used in [30] which is mentioned as a faster method. It is based on inserting the expanded form of m to Eq. (A-18) resulting in the following relation for this parameter

$$m(\gamma) = \gamma - \frac{1}{8}\gamma^2 - \frac{1}{32}\gamma^3 - \frac{11}{1024}\gamma^4 \dots \quad (\text{A-20})$$

It should be noted that $\dot{\psi}_{max} = \dot{\psi}(0) = 2\frac{\sqrt{m}}{\lambda}$ as one of the important parameters of the problem.

The variables ψ , x and z are obtained based on the known parameters of the problem. Now, it is helpful to substitute these functions to obtain f_x as Lagrange multiplier and ε as follows

$$\begin{aligned} f_x &= \kappa \left(\frac{2\pi}{L} \right)^2 \left[1 + \frac{1}{2}\gamma + \frac{9}{32}\gamma^2 + \frac{21}{128}\gamma^3 \dots \right] \\ \varepsilon &= \kappa (2\pi)^2 \frac{L_y^2}{A} \sum_i \frac{b_i \gamma^{i+1}}{i+1} \end{aligned} \quad (\text{A-21})$$

”For any realistic membrane with a finite area compression modulus K_A the jump into nonzero stress at nonzero infinitesimal strain is unrealistic, since initially it is energetically favorable for the membrane to simply reduce the area per lipid; only later will it switch to a curved state beyond the buckling stress of $\kappa (2\pi/L)^2$. [30]”

Because of verification of the results using also the stress in the membrane, it is necessary to express also the stress-strain functions. Deserno *et al.* [30] used orthonormal coordinates $(\mathbf{l}, \mathbf{t}, \mathbf{n})$. If we cut the membrane at every point, there is a tangential direction called \mathbf{t} and the other tangential direction which is perpendicular to the cut called \mathbf{l} . \mathbf{n} is the normal direction in the surface of the membrane. If we consider \mathbf{f} as a force per unit length along the considered cut in the membrane, we have

$$\begin{aligned} \mathbf{f} &= \left[\frac{1}{2}\kappa (K_{\perp}^2 - K_{\parallel}^2) - \sum \right] \mathbf{l} \\ &+ \kappa [K_{\perp\parallel} (K_{\perp} + K_{\parallel})] \mathbf{t} \\ &- \kappa (\nabla_{\perp} K) \mathbf{n} \end{aligned} \quad (\text{A-22})$$

where, K_{\perp} and K_{\parallel} are the local curvatures perpendicular and parallel to the cut, respectively, $K_{\perp\parallel}$ is the off-diagonal element of the local curvature tensor, and ∇_{\perp} is the

directional surface derivative along \mathbf{l} . Now, if we cut the membrane along the direction perpendicular to the plane, we have $K_{\parallel} = K_{\perp\parallel} = 0$ and $K_{\perp} = -\dot{\psi}$. Therefore, Eq. (A-22) can be simplified as follows

$$\mathbf{f} = \left[\frac{1}{2} \kappa \dot{\psi}^2 - \sum \right] \mathbf{l} + \kappa \ddot{\psi} \mathbf{n} \quad (\text{A-23})$$

We can also obtain the compression stress along the x – direction as follows

$$f_x = \mathbf{f} \cdot \mathbf{x} = \left[\frac{1}{2} \kappa \dot{\psi}^2 - \sum \right] \cos \psi - \kappa \ddot{\psi} \sin \psi \quad (\text{A-24})$$

By employing the Euler-Lagrange equation, we can easily find that

$$\sum = -f_x \cos \psi_i \quad (\text{A-25})$$

Henceforth, we want to add the effects of undulations to the presented energy-based model using the procedure described in [30]. The undulations cause wrinkling the buckled membrane. In order to model this behavior as well as shrinkage of the membrane based on the fluctuations, the differences between L corrected by using undulations and L_0 should be accounted in the stress function f_x . The stress-free one-dimensionally varying nearly-flat shape $h(s)$ of the membrane can be expanded in a Fourier series as follows

$$h(x) = \sum_q h_q e^{iqx} \quad \text{with } q \in \frac{2\pi}{L} \mathbb{Z} \text{ and } h_{-q} = h_q^* \quad (\text{A-26})$$

and its energy is given by

$$\varepsilon[h] = L_y \int_0^L dx \left[\frac{1}{2} \kappa [h''(x)]^2 \right] \quad (\text{A-27})$$

In order to obtain $\langle h_q h_q^* \rangle$, necessary for the rest of the procedure, it is required to go one step back. Energy of a membrane under both bending and tension τ can be written as [4]

$$E = \left(\frac{1}{2} \right) \left(\frac{A^2}{4\pi^2} \right) \int d\mathbf{q} (\tau q^2 + \kappa_b q^4) h(\mathbf{q}) h^*(\mathbf{q}) \quad (\text{A-28})$$

In order to go further, let us consider the one-dimensional harmonic oscillator which its energy is governed by $E(x) = k_{sp}x^2/2$ (k_{sp} is spring constant) and its thermal average is

$$\langle E \rangle = k_{sp} \frac{\langle x^2 \rangle}{2} = \left(\frac{k_{sp}}{2} \right) \frac{\int x^2 \exp\left(-\frac{E}{k_B T}\right) dx}{\int \exp\left(-\frac{E}{k_B T}\right) dx} \quad (\text{A-29})$$

Hence, by integrating this equation we can find that $\langle x^2 \rangle = k_B T / k_{sp}$ and $\langle E \rangle = k_B T / 2$. It should be noted that the factor $\int d\mathbf{q}$ is a sum over oscillator modes, with one mode per $(2\pi^2)/A$ in \mathbf{q} -space, each with an energy $(A/2)(\tau q^2 + \kappa_b q^4) h(\mathbf{q}) h^*(\mathbf{q})$. Now, if we consider the average energy of an individual mode is equal to $k_B T / 2$, we obtain

$$\langle h(\mathbf{q}) h^*(\mathbf{q}) \rangle = \frac{k_B T}{A(\tau q^2 + \kappa_b q^4)} \quad (\text{A-30})$$

which in our case becomes

$$\langle h_q h_{q'}^* \rangle = \frac{k_B T}{L_y L \kappa q^4} \delta_{qq'} \quad (\text{A-31})$$

Therefore, the total arc length can be obtained as

$$\begin{aligned} \frac{\langle L_0 \rangle}{L} &= 1 + \frac{1}{2L} \int_0^L dx \langle [h'(x)]^2 \rangle = 1 + \frac{1}{2} \sum_q q^2 \langle |h_q|^2 \rangle \\ &\approx 1 + \frac{L}{2\pi} \int_{L/2\pi}^\infty dq \frac{k_B T L_y L \kappa q^2}{2\pi} =: 1 + \delta \end{aligned} \quad (\text{A-32})$$

where the correction is defined as

$$\delta = \frac{k_B T L}{(2\pi)^2 \kappa L_y} \quad (\text{A-33})$$

Hence, the following relation can be easily obtained to linear order in δ

$$\begin{aligned} \langle L_0 \rangle^{-2} &= L^{-2} [1 - 2\delta + O(\delta^2)] \\ \gamma_0^i &= \gamma^i + i\gamma^{i-1} (1 - \gamma) \delta + O(\delta^2). \end{aligned} \quad (\text{A-34})$$

Finally, we can obtain the following correction for the stress by substituting the corrections into Eq. (A-21) resulting in the following relation

$$\begin{aligned} \delta F_x &= L_y \delta f_x = -\frac{3k_B T}{2L} \sum_{i=0}^{\infty} d_i \gamma^i \\ &= -\frac{3k_B T}{2L} \left[1 + \frac{5}{8}\gamma + \frac{27}{64}\gamma^2 + \frac{295}{1024}\gamma^3 \dots \right] \end{aligned} \quad (\text{A-35})$$

Therefore, the fluctuation correction compared to the ground state result can be written in the lowest order as follows

$$\left| \frac{\delta F_x}{F_x} \right| \sim \frac{3}{8\pi^2} \left(\frac{L}{L_y} \right) \left(\frac{k_B T}{\kappa} \right) \quad (\text{A-36})$$

Bibliography

- [1] Albert B., Johnson A., Lewis J., Raff M., Roberts K., Walter P., *Molecular biology of the cell*, Taylor and Francis Group, 2002.
- [2] Baoukina S., Monticelli L., Risselada H. J., Marrink S. J., Tieleman D. P., *The molecular mechanism of lipid monolayer collapse*, PNAS **105**, 10803-10808(2008).
- [3] Barthes-Biesel D., Diaz A., and Dhenin E., *Efect of constitutive laws for two-dimensional membranes on flow-induced capsule deformation*, J. Fluid Mech. **460**, 211-222(2002).
- [4] Boal D., *Mechanics of the Cell*, Cambridge University Press, Second Edition, 2012.
- [5] Brochard F., Lennon J. F., *Frequency spectrum of the flicker phenomenon in erythrocytes*, J. Phys. Paris **36**, 1035-1047 (1975).
- [6] Canham P. B., *The minimum energy of bending as a possible explanation of the biconcave shape of the human red blood cell*, J. Theoret. Biol. **26**, 61-81 (1970).
- [7] Capovilla R., Guven J., *Stress in lipid membranes*, J. Phys. A. **35**, 6233-6247(2002).
- [8] Chien S., Sung K. P., Skalak R., Usami S., and Aydin Tozeren, *The oretical and expermental studies on viscoelastic properties of erythrocytes membrane*, BioPhys. J. **24**, 463-487(1978).

- [9] Dao M., Lim C. T., Suresh S., *Mechanics of the human red blood cell deformed by optical tweezers*, J. Mech. Phys. Solids **51**, 2259-2280(2003).
- [10] Dembo M., Torney D. C., Saxman K., Hammer D., *The reaction-limited kinetics of membrane-to-surface adhesion and detachment*, Proc. R. Soc. Lond. B **234**, 55-83 (1988).
- [11] Do N. T., *Investigating peptide/RNA binding in anti-HIV research by molecular simulations: Electrostatic recognition and accelerated sampling*, Thesis, SISSA (2012).
- [12] Domokos G., Fraser W. B., Szeberenyi I., *Symmetry-breaking bifurcation of the uplifted elastic strip*, Physica D **185**, 67-77(2003).
- [13] Duwe H. P., Kaes J., and Sackmann E., *Bending elastic moduli of lipid bilayers: modulation by solutes*, J. Phys. France. **51**, 945-962 (1990).
- [14] Ethier C. R., Simmons C. A., *Introductory biomechanics: From cells to organisms*, Cambridge University Press, First Edition, 2007.
- [15] Evans E. A., *New membrane concept applied to analysis of fluid shear-deformed and micropipet-deformed red blood cells*, Biophys. J. **13**, 941-954(1973).
- [16] Evans E. A., Skalak R., *Mechanics and thermal dynamics of biomembranes*, CRC Press Inc. (1980).
- [17] Evans E., Rawicz W., *Entropy-driven tension and bending elasticity in condensed-fluid membranes*, Phys. Rev. Lett., **64**, 2094-2097 (1990).
- [18] Evans E. A. and Waugh R., *Osmotic correction to elastic area compressibility measurements on red cell membrane*, Biophys. J. **20**, 307-313 (1977).
- [19] Evans E., *Bending elastic modulus of red blood cell membrane derived from buckling instability in micropipet aspiration test*, Biophys. J. **43**, 27-30 (1983).

- [20] Fisseha D., Katiyar V. K., *Analysis of mechanical behavior of red cell membrane in sickle cell disease*, Appl. Math. **2**, 40-46(2012).
- [21] Fournier J. B., Galatola P., *Critical fluctuations of tense fluid membrane tubules*, Phys. Rev. Lett. **98**, 8103-8106(2007).
- [22] Fredberg J. J., Stamenovic D., *On the imperfect elasticity of lung tissue*, J. Appl. Physiol. **67**, 2408-2419(1989).
- [23] Gao Y., Hoo Fatt M. S., *Dynamic pulse buckling of single curvature composite shells under external blast*, Thin Wall. Struct. **52**, 149-157(2012).
- [24] Golubovic L., Moldovan D., and Peredera A., *Dynamics of the Euler buckling instability*, Phys. Rev. Lett. **81**, 3387-3390(1998).
- [25] Helfrich W., *Elastic properties of lipid bilayers: theory and possible experiments*, Z. Naturforsch. **28c**, 693-703 (1973).
- [26] Henon S., Lenormand G., Richert A., Gallet F., *A new determination of the shear modulus of the human erythrocyte membrane using optical tweezers*, Biophys. J. **76**, 1145-1151(1999).
- [27] Herant M., Heinrich V., Dembo M., *Mechanics of neutrophil phagocytosis: experiments and quantitative models*, J. Cell Sci. **119**, 1903-1913 (2005).
- [28] Hochmuth R. M., *Properties of red blood cells. In handbook of Bioengineering*, McGraw-Hill Inc., eds. Skalak R. and Chien S., 1982.
- [29] Hochmuth R. M., Wiles H. C., Evans E. A., and Mccown J. T., *Extensional flow of erythrocyte membrane from cell body to elastic tether II. Experiment*, BioPhys. J. **39**, 83-89(1982).
- [30] Hu M., Diggins P., and Deserno M., *Determining the bending modulus of a lipid membrane by simulating buckling*, J. Chem. Phys. **138**, 214110(2013).

- [31] Jay A. W. L., *Viscoelastic properties of the human red blood cell membrane 1. Deformation, volume loss, and rupture of red cells in micropipettes*, Biophys. J. **13**, (1973).
- [32] Jay A. W. L. and Canham P. B., *Viscoelastic properties of the human red blood cell membrane II. area and volume of individual red cells entering a micropipette*, Biophys. J. **17**, (1977).
- [33] Kenny S., Pegg N., Taheri F., *Finite element investigations on the dynamic plastic buckling of a slender beam subject to axial impact*, Int. J. Impact Eng. **27**, 179-195(2002).
- [34] King M. R., Hammer D. A., *Multipartical adhesive dynamics: Hydrodynamic recruitment of rolling leukocytes*, Proc. Natl. Acad. Sci. USA. **98**, 14919-14924 (2001).
- [35] Koenig B. W., Strey H. H., and Gawrisch K., *Membrane lateral compressibility determined by NMR and X-ray diffraction: effect of acyl chain unsaturation*, Biophys. J. **73**, 1954-1966 (1997).
- [36] Landau L. D., Lifshitz E. M., *Theory of elasticity*, Butterworth-Heinemann, Third Edition, 1999.
- [37] Lee A. G., *Biomembranes*, JAI Press Inc., 1995.
- [38] Lee M. H., Wu P. H., Staunton J. R., Ros R. T., Longmore G. D., and Wirtz D., *Mismatch in mechanical and adhesive properties induced pulsating cancer cell migration in epithelial monolayer*, Biophys. J. **102**, 2731-2741 (2012).
- [39] Lidmar J., *Virus shapes and buckling transitions in spherical shells*, Phys. Rev. E. **68**, 1910-1919(2003).
- [40] Maleki M., Madani Tonekaboni S. A., Abbasbandy S., *A Homotopy Analysis Solution to large deformation of beams under static arbitrary distributed load*, Appl. Math. Model., Ms. Ref. No.: amm 12379R1.

- [41] Mills J. P., Qie L., Dao M. Lim C. T., and Suresh S., *Nonlinear elastic and viscoelastic deformation of the human red blood cell with optical tweezers*, MCB **1**, 169-180(2004).
- [42] Milner S. T., Joanny J. F., Pincus P., *Buckling of Langmuir monolayers*, Europhys. Lett. **9**, 495-500(1989).
- [43] Mutz M., Helfrich W., *Bending rigidities of some biological model membranes as obtained from the Fourier analysis of contour sections*, J. Phys. France.**51**, 991-1002 (1990).
- [44] Nagle J., Tristram-Nagle S., *Structure of lipid bilayers*, Biochim. Biophys. Acta **1469**, 159-195 (2000).
- [45] Needham D., Nunn R. S., *Elastic deformation and failure of lipid bilayer membranes containing cholesterol*, Biophys. J. **58**, 997-1009 (1990).
- [46] Noguchi H., *Anisotropic surface tension of buckled fluid membranes*, Phys. Rev. E **83**, 1919-1925 (2011).
- [47] Noguchi H., *Solvent-free coarse-grained lipid model for large-scale simulations*, J. Chem. Phys. **134**, 5101-5112(2011).
- [48] Noguchi H., and Gompper G., *Shape transitions of fluid vesicles and red blood cells in capillary flows*, Proc. Natl. Acad. Sci. USA. **102**, 14159-14164 (2005).
- [49] Noguchi H., and Gompper G., *Meshless membrane model based on the moving least-squares method*, Phys. Rev. E. **73**, 1903-1914(2006).
- [50] Noguchi H., and Gompper G., *Dynamics of vesicle self-assembly and dissolution*, J. Chem. Phys. **125**, 4908-4920(2011).
- [51] Otter W. K. D., *Area compressibility and buckling of amphiphilic bilayers in molecular dynamics simulations*, J. Chem. Phys. **123**, 4906-4914(2005).

- [52] Peterson M. A., Strey H., and Sackmann E., *Theoretical and phase contrast microscope eigenmode analysis of erythrocyte flicker: amplitudes*, J. Phys. II France **2**, 1273-1285 (1992).
- [53] Pocivavsek L., Dellsy R., Kern A., Johnson S., Lin B., Lee K. Y. C., Cerda E., *Stress and fold localization in thin elastic membrane*, Science **320**, 912-916(2008).
- [54] Pocivavsek L., Frey S. L., Krishan K., Gavrilov K., Ruchala P., Waring A. J., Walther F. J., Dennin M., Witten T. A., Lee K. Y. C., *Lateral stress relaxation and collapse in lipid monolayers*, Soft Matter **4**, 2019-2029(2008).
- [55] Puig-de-Morales-Marinkovic M., Turner K. T., Butler J. P., Fredberg J. J., and Suresh S., *Viscoelasticity of the human red blood cell*, Am J. Physiol. Cell Physiol. **293**, C579-C605(2007).
- [56] Rand R. P., *Mechanical properties of the red cell membrane: II. Viscoelastic breakdown of the membrane*, Department of Physics, University of Western Ontario, 1964.
- [57] Rawicz W., Olbrich K. C., McIntosh T., Needham D., and Evans E., *Effects of chain length and unsaturation on elasticity of lipid bilayers*, Biophys. J. **79**, 328-339 (2000).
- [58] Sherwood L., Klandorf H., Yancy P. H., *Animal Physiology*, Brooks/Cole, Second Edition, 2013.
- [59] Shiba H., Noguchi H., *Estimation of the bending rigidity and spontaneous curvature of fluid membranes in simulations*, Phys. Rev. E. **84**, 1926-1938(2011).
- [60] Singer S. J., and Nicholson G. L., *The fluid mosaic model of the structure of cell membranes*, Science **175**, 720-731 (1972).
- [61] Skalak R., Tozeren A., Zarda R. P., and Chien S. *Strain energy function of red blood cell membranes*, Biophys. J. **13**, 245-264(1973).
- [62] Smith C. A., Wood E. J., *Cell biology*, Chapman and Hall, Second edition, 1996.

- [63] Sollic P., *Inmolecular gels-materials with self-assembled fibrillar networks*, Springer (Netherlands), ed. by R. G. Weiss, P. Terech (2006).
- [64] Sukumaran S., Seifert U., *Influence of shear flow on vesicles near a wall: a numerical study*, Phys. Rev. E. **64**, 11916-11927 (2001).
- [65] Suresh S., *Biomechanics and biophysics of cancer cells*, Acta Biomater. **3**, 413-438 (2007).
- [66] Thews G., Mutschler E., Vaupel P., *Human anatomy, physiology and Pathophysiology*, Cambridge University Press, English Language Edition, 1985.
- [67] Timoshenko S., Goodier J. N., *Theory of elasticity*, Butterworth-Heinemann, First Edition, 1951.
- [68] Tozeren A., Byers S. W., *New biology for Engineers and Computer Scientists*, Pearson Education Inc., 2004.
- [69] Tozeren A., Skalak R., Sung K. P., Chien S., *Viscoelastic behavior of erythrocyte membrane*, BioPhys. J. **39**, 23-32(1982).
- [70] Verdier C., Etienne J., Duperray A., Preziosi L., *Rheological properties of biological materials*, C. R. Acad. Sci.-Physics , 1-21 (2009).
- [71] Vliementhart G. A., and Gommer G., *Forced crumpling of self-avoiding elastic sheets*, Nature Mater. **48**, 216-221(2006).
- [72] Wirtz D., Konstantopoulos K., and Searson P. C., *The physics of cancer: the role of physical interactions and mechanical forces on metastasis*, Nat. Rev. Cancer **11**, 512-522 (2011).
- [73] Witten T. A., *Stress focusing in elastic sheets*, Rev. Mod. Phys. **79**, 643-675(2007).
- [74] Xi F., Liu F., Li Q. M., *Large deflection response of an elastic, perfectly plastic cantilever beam subjected to a step loading*, Int. J. Impact Eng. **48**, 33-45 (2012).

- [75] Yeoh O. H., *Characterization of elastic properties of carbon-black-filled rubber vulcanizates*, Rubber Chem. Tech. **63**, 792-805(1990).
- [76] Yin J., Cao Z., Li C., Sheinman I., Chen X., *Stress-driven buckling patterns in spheroidal core/shell structures*, PNAS **105**, 19132-19135(2008).
- [77] Zhang Q., and Witten T. A., *Microscopic wrinkles on supported surfactant monolayers*, Phys. Rev. E. **76**, 1608-1620(2007).
- [78] Zilker A., Ziegler M., and Sackmann E., *Spectral analysis of erythrocyte flickering in the $0.3 - 0.4\mu\text{m}^{-1}$ regime by microinterferometry combined with fast image processing*, Phys. Rev. A. **46**, 7998-8001 (1992).